| | |
|---|---|
| Title: | **Experimental Methods in Polymer Science: Modern Methods in Polymer Research & Technology** |
| By: | T. Tanaka, ed. |
| ISBN: | 0 126 83265 x |
| Publisher: | Academic Press |
| Copyright: | 2000 |
| Page Count: | 616 |
| Trim Size: | |
| Format: | Hardcover |

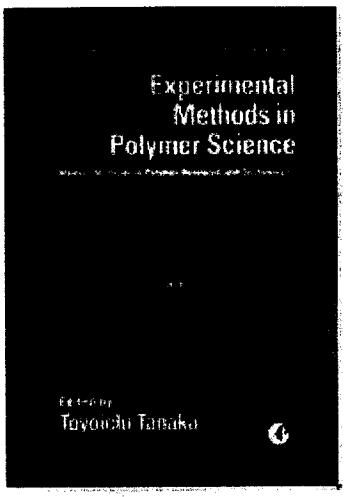


1 Add to cart Back View Cart

Keywords associated with this title:

Design of Experiments
Laboratory Manuals
Polymer Science
Spectroscopy and Spectrometry
Surface Physics
Test Methods

Successful characterization of polymer systems is one of the most important objectives of today's experimental research of polymers. This practical resource addresses the most important techniques used in this field of research; it covers principles, practical techniques, and actual examples, presenting ideas and methods from an international perspective. It can be used as a handbook or as a lab manual for both students and researchers.

From the Preface: "Polymers are considered among the most important materials in science and technology for the 21st century. The uses of polymers in our everyday life are being extended and diversified day by day. The chemical, medical, and agricultural industries as well as many others are heavily dependent on a wide variety of polymers. Moreover, polymers are the materials that nature chose as the vehicle for life that appeared on this earth..."

Target Audience: Any scientist or engineer who wishes to be able to execute experimental research in polymers using modern methods.

# Chapter 5 | Mechanical Spectroscopy of Polymers

M. Mours

*BASF AG, Ludwigshafen*
*Germany*

H. H. Winter

*Department of Chemical Engineering*
*University of Massachusetts at Amherst*
*Amherst, Massachusetts*

## 5.1 Introduction

We all have bounced balls and can remember differences between the bouncing of balls for soccer, basketball, tennis, golf, or billiards. Balls bounce differently when thrown hard at a surface or when just dropped. Bouncing is an informative experiment but not very controlled in its course. Mechanical spectroscopy (MS) can be viewed as a sophisticated bouncing experiment in which a material sample, most commonly in the shape of a small disk or a rectangular sheet, is deformed under a periodic load. The material can be elastic (like the bouncing ball), but the test also applies to viscous fluids because deformation and restoration of the original shape are both prescribed by the experiment.

Mechanical spectroscopy is able to probe the dynamics of relaxation processes for liquids and solids in their equilibrium state. The applied stress or strain needs to be small enough so that perturbations of the equilibrium structure can safely be neglected.

Relaxation processes in polymers occur on a wide range of time scales. Fast dynamics is associated with small-scale relaxation processes (small molecules, molecular strands, subunits of molecules) and, vice versa, slow dynamics belongs to macromolecular motions or long-range correlation of supermolecular motions (physical aggregation, for instance). To appreciate the wide interest in MS, it is important to realize that the time dependence of isochoric rheology is completely described by a single material function, the relaxation time spectrum $H(\lambda)$, and that MS is the most advanced method of determining $H(\lambda)$. The shape of $H(\lambda)$ is often correlated with specific molecular architectures. The spectrum's sensitivity to small changes in molecular connectivity makes it a powerful tool to distinguish small differences in otherwise undistinguishable materials. Systematic patterns have been



EXPERIMENTAL METHODS
IN POLYMER SCIENCE


ISBN 0-12-683265-X/$30.00

found in $H(\lambda)$ that are useful for developing polymers of novel molecular architecture or for tailoring polymers to specific applications. Recent successes include discoveries of the relaxation time spectrum of the critical gel (polymer at its gel point) and of the spectrum of long, linear, flexible molecules of uniform molecular weight.

Mechanical spectroscopy is a mature experimental technique. Excellent commercial instruments are available for measuring the necessary data to determine $H(\lambda)$, and computer methods are readily available to analyze the data. However, the high sensitivity of the experiment makes it prone to artifacts. It is necessary to understand MS to gain full access to its potential.

### *5.1.1 RHEOLOGY OF THE EQUILIBRIUM STATE*

Before proceeding, several basic viscoelastic parameters of polymeric liquids and solids need to be defined. This can be done most easily with the stress relaxation experiment (Figure 5.1) in which a small shear strain $\gamma_0$ is imposed on an

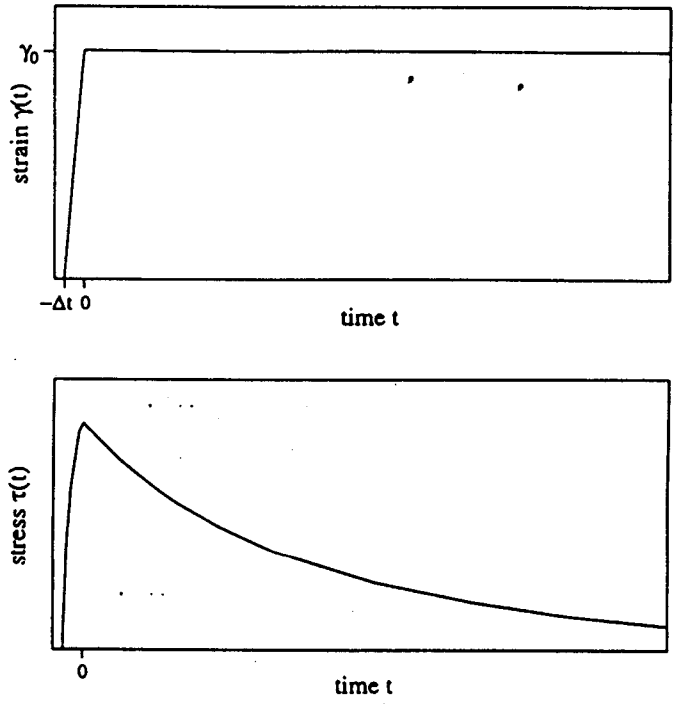


Figure 5.1 Dynamics of the stress relaxation experiment. A finite strain $\gamma_0$ is applied rapidly by shearing during a short time interval $\Delta t$. The resulting stress $\tau(t)$ is measured over a long time.

equilibrated material sample while the shear stress response as a function of time is measured. The stress in the sample rises when $\gamma_0$ is applied at the beginning of the experiment, but then it relaxes as $\gamma_0$ is kept constant. Instead of plotting the decaying shear stress $\tau(t)$ (Figure 5.1), one most commonly plots the ratio of stress and strain, called the relaxation modulus $G(t, \gamma_0)$. Data are shown for a polyethylene melt in Figure 5.2. Stress relaxation data at very small strain (linear viscoelastic limit) collapse into a single time function

$$\overset{0}{G}(t) = \tau(t)/\gamma_0 \tag{1}$$

represented by the top curve in Figure 5.2. The linear relaxation modulus $\overset{0}{G}(t)$ is independent of the applied strain.

The dynamics of the equilibrium state has significance for the nonequilibrium state (large strain). For a polymeric liquid, as shown here, Einaga *et al.* [2] discovered that large shear strains cause the time function $\overset{0}{G}(t)$ to shift vertically

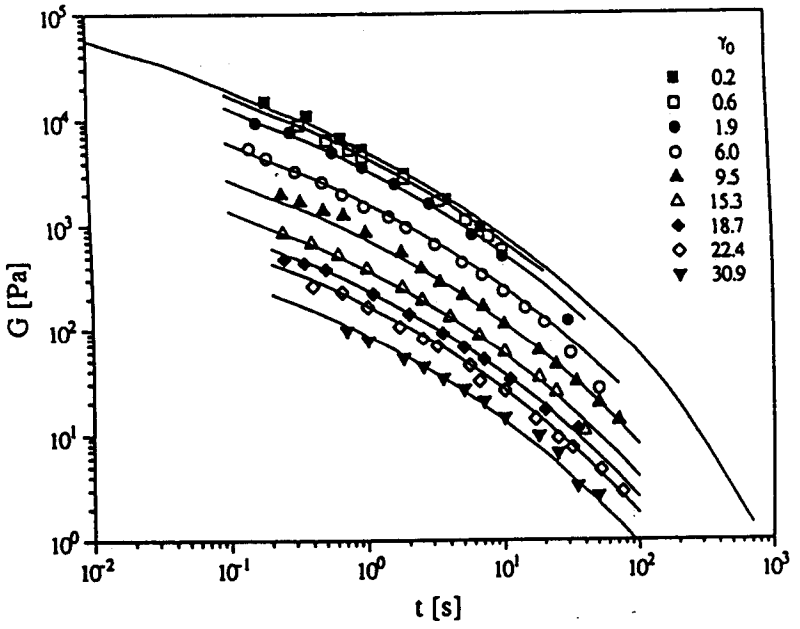


**Figure 5.2** Strain dependence of the relaxation modulus $\overset{0}{G}(t)$ of a molten polyethylene. Data replotted from [1]. The top line represents the relaxation modulus calculated from the spectrum. The other lines were shifted vertically to obtain the best possible fit for each experimental data set.

to lower values

$$G(t, \gamma_0) = \overset{0}{G}(t)\, h(\gamma_0), \tag{2}$$

however, without changing its shape: time effects and strain effects can be expressed as a product of two separate functions. Many materials have been found to exhibit this phenomenon (when probed at long time scales [3]). This observation has important consequences for the modeling of molecular dynamics. The magnitude of the shift $h(\gamma_0)$ describes the effect of large strains [4, 5]. This chapter will only discuss the small strain behavior, i.e., the viscoelasticity of the equilibrium state.

Rheological experiments are quite limited in the range of time scales they can access at once. The polyethylene melt (Figure 5.2) was probed at relatively large time scales at which all its short modes had already relaxed. A more complete relaxation modulus would include glassy modes, as shown schematically in Figure 5.3, in which curve (a) represents a typical polymer melt. Distinct regions can be identified that are characterized by their own molecular dynamics. At very short times, the polymer can only relax on a very small scale. It is in its glassy state. Given more time, a gradual transition (glass transition) occurs towards the

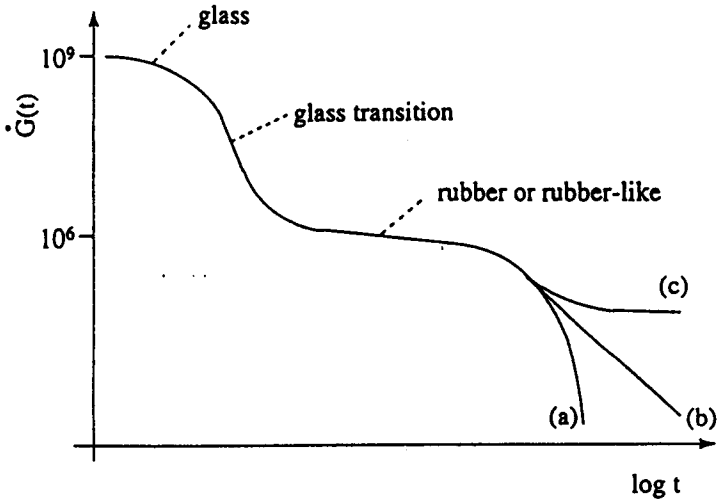


**Figure 5.3** Schematic of the relaxation modulus of polymer melts (a), polymer critical gels (b), and solid polymers (c). The critical gel is the material at the transition from liquid to solid.

rubbery state. For polymer melts, the time scale of rubbery behavior is called the entanglement region. At even longer times, the polymer melt, curve (a), has time to flow. The flow region is also called the terminal region because no longer time scales beyond $\lambda_{max}$ are present in the polymer.

### 5.1.2 SOLIDS VERSUS LIQUIDS

The relaxation modulus is defined for liquids and for solids. The stress of the polymeric liquid of Figure 5.2 relaxes to zero, as is typical for a liquid. In the case of a solid (curve (c) in Figure 5.3), the stress can only decay to a finite value that corresponds to the equilibrium modulus $G_e$. The nonrelaxing stress contributions of a solid in the preceding stress relaxation experiment would be

$$\lim_{t\to\infty} \tau = G_e\gamma_0 \tag{3}$$

Even solids have transient relaxation modes. The longest relaxation time of these modes is finite. In this chapter on MS, we are mostly concerned with transient stress contributions $\overset{0}{G}(t) - G_e$ and treat $G_e$ as an independent material parameter, which is zero for liquids and finite for solids.

An ideal solid would show no stress relaxation at all, that is, $\tau(t) = G_e\gamma_0 =$ constant. The longest relaxation time is vanishingly small.

At the transition from liquid to solid, stress relaxes in a power law (see curve (b) in Figure 5.3). The transition state (critical gel) has its own relaxation pattern, which is universal [6, 7].

### 5.1.3 BOLTZMANN EQUATION OF LINEAR VISCOELASTICITY

The relaxation modulus $\overset{0}{G}(t)$ is the only material function required to calculate the stress $\tau(t)$ as a function of any strain history $\dot{\gamma}(t')$ for $-\infty < t' < t$ as long as the strain is small enough to avoid perturbation of the equilibrium state of the material. The extra stress in the equilibrium material is fully defined by the classical theory of linear viscoelasticity of Boltzmann (see, for example, [8]):

$$\tau(t) = \int_{-\infty}^{t} dt' \, \overset{0}{G}(t - t')\,\dot{\gamma}(t') \tag{4}$$

The variable $t - t'$ denotes the distance into the past, where $t$ is the current time and $t'$ is an instant in the past.

### 5.1.4 RELAXATION TIME SPECTRUM

The relaxation modulus can be expressed as a Laplace transform of a continuous relaxation time spectrum $H(\lambda)$:

$$\overset{0}{G}(t) = G_e + \int_0^\infty \frac{d\lambda}{\lambda} H(\lambda)\, e^{-t/\lambda} \tag{5}$$

$H(\lambda)$, called the spectrum from here on, is an alternative to the directly observable relaxation modulus $\overset{0}{G}(t)$. Each of these material functions alone is sufficient for describing the viscoelastic behavior of a material. The equivalent Boltzmann equation for $H(\lambda)$ is given in Appendix 5.A.

The $H(\lambda)$ expresses the distribution of relaxation strengths as a function of the relaxation time $\lambda$. It is a positive-valued function that is finite in the range $0 < \lambda < \lambda_{max}$ and zero above the longest relaxation time $\lambda_{max}$. The longest relaxation time $\lambda_{max}$ belongs to the largest correlation length in the material (= entire molecule in a polymer melt or largest defect in a polymeric solid).

The spectrum $H(\lambda)$ cannot be measured directly. It is preferably obtained through mechanical spectroscopy and it requires extensive data analysis, resulting in a discrete spectrum (see Section 5.3). Most physical models of materials are expressed in discrete spectra, and it is not clear yet whether $H(\lambda)$ is really continuous or discrete.

Molecular models for relaxation time spectra based on molecular theory were introduced by Rouse [9], de Gennes [10], and Doi and Edwards [11]. The models start out with the most simple molecular geometry, that of long, linear, flexible chains of uniform length. Predictions from these initial theories compare well with experimental data of polymers within narrow time domains, but theories need to become quite sophisticated for covering a wider range of relaxation times [11–14].

Many empirical models have also been proposed [71]. A recent proposal for the relaxation of long, linear, flexible molecules of nearly uniform length gives very good agreement with measured data [15]. This so-called BSW spectrum (of Baumgärtel, Schausberger and Winter)

$$H(\lambda) = \begin{cases} n_e G_N^0 \left[ \left(\frac{\lambda}{\lambda_c}\right)^{-n_1} + \left(\frac{\lambda}{\lambda_{max}}\right)^{n_e} \right] & \text{for } \lambda < \lambda_{max} \\ 0 & \text{for } \lambda_{max} < \lambda \end{cases} \tag{6}$$

comprises a superposition of two power laws, the first one describing the self-similarity of the glass transition and the second one expressing the self-similarity of the entanglement behavior. The material parameter $G_N^0$ is the plateau modulus,

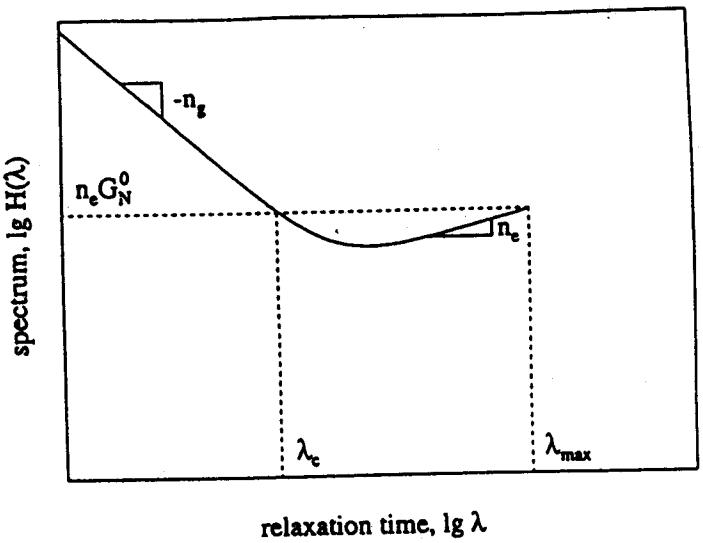


**Figure 5.4** Schematic of the BSW spectrum. The two power laws with slopes $-n_g$ and $n_e$ correspond to the glass transition and entanglement relaxation regime, respectively. The $\lambda_c$ is the crossover relaxation time from entanglement to glass transition. The longest relaxation time $\lambda_{max}$ belongs to the relaxation of the entire chain. The power laws are an expression of the self-similarity of the polymer chain's, $n_e$, and of the glassy superstructure, $n_g$.

$n_g$ and $n_e$ are the relaxation exponents in the glass transition and entanglement regime, respectively, $\lambda_c$ is the characteristic time of crossover to the glass transition, and $\lambda_{max}$ is the longest relaxation time. A schematic of the BSW spectrum is presented in Figure 5.4. Generic parameter sets can be evaluated for materials with similar molecular architecture but different molecular weights $M$ [16]. The only molecular-weight-dependent parameter is the longest relaxation time

$$\lambda_{max} = \lambda_c \left(\frac{M}{M_c}\right)^z \tag{7}$$

which compares $M$ to the polymer-specific crossover molecular weight $M_c$ for the onset of entanglements. Exponent $z$ is the scaling exponent that also describes the dependence of zero-shear viscosity on molecular weight [8]; experimentally $z$ was found to have values of about 3.4 for large molecules $M \gg M_c$ [17]. The BSW spectrum is the simplest spectrum known to be able to express relaxation data of polymers with linear flexible molecules of uniform molecular weight. It has been serving as reference when studying more complicated materials.

### 5.1.5 DISCRETIZED FORM OF MODULUS AND SPECTRUM

Discrete spectra result in a relaxation modulus

$$\overset{0}{G}(t) = G_e + \sum_{i=1}^{N} g_i e^{-t/\lambda_i} \tag{8}$$

where coefficients $g_i$ and relaxation times $\lambda_i$ are material parameters. Here, we chose the sum of $N$ exponential decays (Maxwell modes) for the time dependence of the material. This does not pose any lack of generality because any continuous function $\overset{0}{G}(t)$ may be approximated by such a discrete set of Maxwell relaxation modes. It should be noted that the discrete relaxation time spectrum

$$H(\lambda) = \sum_{i=1}^{N} g_i \, \delta(\lambda/\lambda_i - 1) \tag{9}$$

is governed by the same parameter set $g_i, \lambda_i, i = 1, 2, 3, \ldots N$ as the relaxation modulus. The expression $\delta(y)$ is the Dirac delta function.

Figure 5.5 shows the discrete relaxation and retardation time spectrum for a linear polybutadiene with a weight-average molecular weight Mw = 70,000. At the same time, the calculated material functions $\overset{0}{G}(t)$ and $\overset{0}{J}(t)$ are displayed as solid lines. The compliance $\overset{0}{J}(t)$ will be defined next.

### 5.1.6 RETARDATION TIME SPECTRUM

The stress relaxation experiment is only one of many ways of defining and measuring viscoelasticity in materials. Another useful approach requires application of a constant stress $\tau_0$ on the material while the resulting strain $\gamma(t)$ is measured. This is the so-called creep experiment. The resulting strain is commonly expressed as compliance

$$\overset{0}{J}(t) = \gamma(t)/\tau_0 \tag{10}$$

or as retardation time spectrum $L(\lambda)$ [8]. All such related viscoelastic functions can be converted into each other [18]. If, for instance, the relaxation time spectrum is known, it is possible to convert it to the retardation time spectrum; there is a one-to-one relation between these two types of spectra [8]:

$$L(\lambda) = \frac{H(\lambda)}{\left(G_e - \int_0^\infty \frac{du}{u} \frac{H(u)}{\lambda/u - 1}\right)^2 + \pi^2 H(\lambda)^2} \tag{11}$$

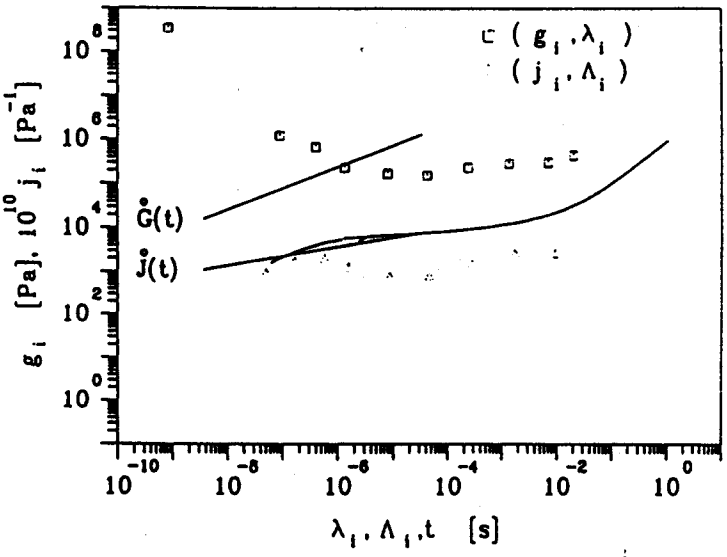


**Figure 5.5** Discrete relaxation time spectra $g_i, \lambda_i$ and retardation time spectra $j_i, \Lambda_i$ for a polybutadiene (symbols). These spectra were used to calculate the relaxation modulus $\overset{0}{G}(t)$ and the compliance $\overset{0}{J}(t)$ (lines). The values of $g_i$ and $j_i$ depend on the spacing of the discrete modes.

It would exceed the scope of this chapter to establish the wide range of such relations. The focus will be on the relaxation modulus and the relaxation time spectrum because either one, by itself, already defines the viscoelasticity polymeric liquids and solids.

### *5.1.7 SCOPE OF MECHANICAL SPECTROSCOPY*

Mechanical spectroscopy (MS) determines the above material properties by probing specific material samples in small amplitute oscillation at prescribed frequency $\omega$. MS quantifies the strength, time scale, and temperature dependence of the characteristic relaxation modes of a material. Most advantageous is its ability to detect and resolve small differences between materials and to express changes in materials during cross-linking or melting (to name some typical examples). Mechanical spectroscopy is used for developing new materials and for tailoring their processing behavior.

Mechanical spectroscopy applies a periodic strain to the material. This has several important advantages compared with other techniques:

1. Each data point is dominated by the specific relaxation modes with relaxation times near $\lambda = 1/\omega$. Other relaxation modes have less influence.
2. The experimental time for taking a single data point (sampling time) is about $t_S = 2\pi/\omega$ independent of any longer relaxation modes that might be present in the sample.
3. Each of the dynamic moduli independently carries all the information about the spectrum.

As an introduction we used step strain behavior to demonstrate the relaxation properties of materials in a most obvious way. For determining relaxation properties, however, the time-periodic experiment of MS is preferable. It will be discussed next.

## 5.2 Mechanical Spectroscopy Experiment

### *5.2.1 SHEAR FLOW NOTATION*

For the purpose of MS, which conventionally is performed in shear rheometers, it is sufficient to consider $\tau(t)$ to be the shear stress in response to a shearing deformation at a shear rate

$$\dot{\gamma}(t') = \frac{\partial}{\partial t'}\gamma(t; t') \tag{12}$$

over the history of the material, $-\infty < t' < t$. The restriction to shear flow does not cause any loss of generality (in isotropic materials at small strains, equilibrium state) because the same spectrum governs all flows and deformations in the linear viscoelastic range, i.e. the spectrum $H(\lambda)$ is equally applicable to other types of deformations (extension, for instance) within the linear viscoelastic range, as will be shown in Section 5.6.

The stress components for the shear experiment are shown in Figure 5.6. These are the shear stress

$$\tau(t) \equiv \tau_{21} \tag{13}$$

which we will simply call $\tau$ in the context of this discussion of MS, and the normal stress differences

$$N_1 = \tau_{11} - \tau_{22} \tag{14}$$

$$N_2 = \tau_{22} - \tau_{33} \tag{15}$$

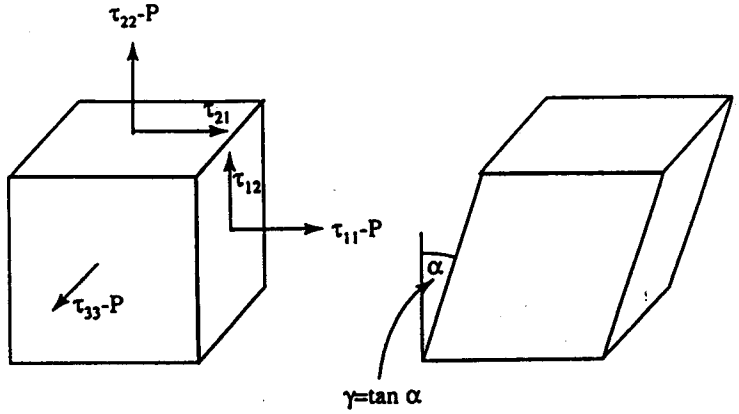


Figure 5.6 Infinitesimal material element in shear, where 1 is the velocity direction, 2 is the velocity gradient direction, and 3 is the vorticity direction. The material element is shown at two times, $t'$ and $t$; $\gamma(t; t')$ is the shear strain.

Normal stresses and the shear stress are governed by the same relaxation modulus and spectrum, i.e., MS can concentrate on measurement of the shear stress only. Normal stresses and pressure $P$ do not contribute directly.

### 5.2.2 *OSCILLATORY SHEAR*

The MS experiment is performed by placing the viscoelastic material (test sample) in a mechanical device (rheometer) that allows small-amplitude sinusoidal shearing at a strain

$$\gamma(t) = \gamma_0 \sin(\omega t); \quad \text{or} \quad \text{a strain rate } \dot{\gamma}(t) = \omega\gamma_0 \cos(\omega t) \tag{16}$$

After some start-up time (in the order of $1/\omega$), the stress in the sample responds sinusoidally

$$\begin{aligned} \tau(t) &= \tau_0 \sin(\delta + \omega t) \\ &= G'(\omega)\,\gamma_0 \sin(\omega t) + G''(\omega)\,\gamma_0 \cos(\omega t) \end{aligned} \tag{17}$$

(see Figure 5.7). The frequency of the sinusoidal stress $\tau(t)$ is the same as that of the strain $\gamma(t)$; however, $\tau(t)$ is shifted by a phase angle $\delta(\omega)$. The factor $\tau_0(\omega, \gamma_0)$ is the amplitude of the sinusoidal stress. The angular frequency $\omega = 2\pi f$ [rad/s] is defined by the number of cycles per time given by the frequency $f$ [Hz]. For the data analysis, it does not matter whether the strain is prescribed and the stress is responding, or vice versa. Both types of mechanical spectrometers are equally common.

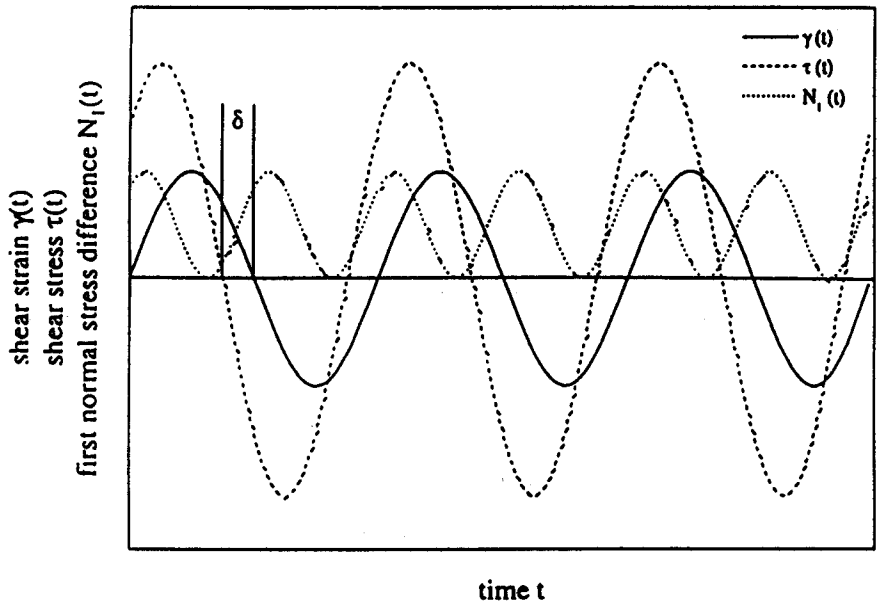


**Figure 5.7** Schematic of the imposed strain function $\gamma(t)$ and the material response (shear stress $\tau(t)$ and first normal stress difference $N_1(t)$) in a small-amplitude oscillatory shear experiment.

Mechanical spectroscopy derives its name from the fact that the sample is probed at prescribed time scales $t \approx 1/\omega$ that depend on the choice of the experimental frequency. The experiment is repeated for a range of frequencies, $\omega_{min} < \omega < \omega_{max}$. Because of experimental constraints (e.g., weak torque values at low frequencies or large slip and inertial effects at high frequencies), it is usually impossible to measure $G'(\omega)$ and $G''(\omega)$ with a commercial rheometer directly over more than three or four decades of frequency.

It is customary to decompose the stress (Eq. (17)) into a part that is in phase with the sinusoidal strain (Eq. (16)) governed by the storage modulus

$$G'(\omega) = \frac{\tau_0}{\gamma_0} \cos\delta \tag{18}$$

and a 90° out-of-phase part governed by the loss modulus

$$G''(\omega) = \frac{\tau_0}{\gamma_0} \sin\delta \tag{19}$$

The objective of the oscillatory shear experiment is to determine these two material-specific moduli over a wide range of frequency, temperature, pressure, or other

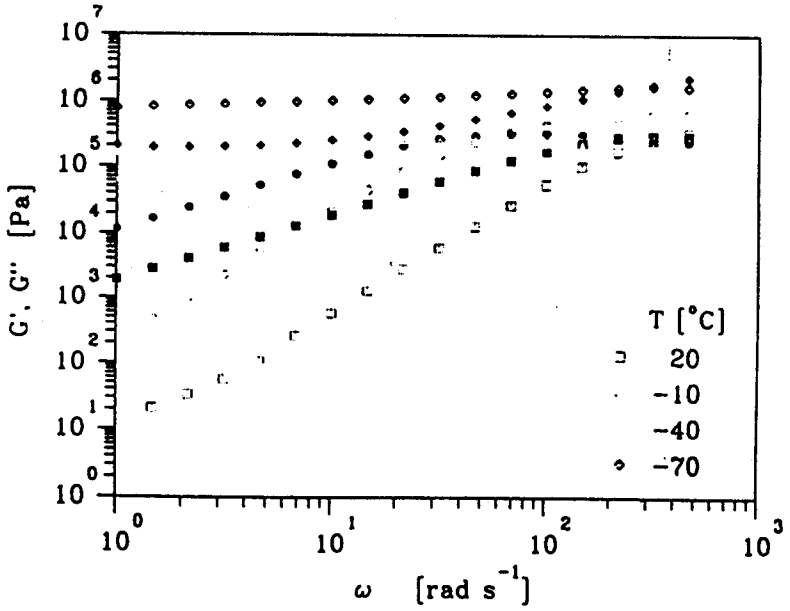


**Figure 5.8** Dynamic moduli measured at different temperatures as used for the construction of the master curve shown in Figure 5.21 by time–temperature superposition. Open symbols represent $G'$; filled symbols represent $G''$. Data from Mours and Winter 1994 [19].

material-affecting parameters. The frequency-dependent moduli are generally valid for liquids and solids, i.e., for any isotropic material as long as the strain amplitude $\gamma_0$ is sufficiently small. $G'$ is a measure of the stored energy and $G''$ of the dissipated energy per cycle.

A typical data set (see Figure 5.8), spans about three to four decades in frequency. The frequency range can be extended by time–temperature superposition [8], which will be discussed in Section 5.5.1.

### 5.2.3 *MULTIWAVE TECHNIQUES [20]*

Instead of probing samples with a single frequency at a time (or a sequence of single frequencies), it is possible to apply $m$ frequencies simultaneously

$$\gamma(t) = \sum_{j=1}^{m} \gamma_j \sin(\omega_j t) \tag{20}$$

and decompose the stress response

$$\tau(t) = \sum_{j=1}^{m} \tau_j \sin(\delta_j + \omega_j t) \tag{21}$$

into $m$ individual components. The frequency is the same for corresponding components of strain and stress. The result of the experiment is a set of $m$ dynamic moduli $G'(\omega_j)$, $G''(\omega_j)$ that are then evaluated as if each of them were being measured in a conventional (single-frequency) experiment. The number of probing modes $m$ cannot be very high, for the sum of the strain amplitudes

$$\gamma_{max} = \sum_{j=1}^{m} \gamma_j \tag{22}$$

should not exceed the linear viscoelastic limit. Typically one may choose $m = 3$.

The multiwave technique saves experimental time because, while measurements are being made at the lowest frequency appropriate for a specific test sample, several higher frequencies may be run simultaneously. Preferably, the lowest experimental frequencies are probed together to save the most time. Such time savings are especially important for the study of transient materials that change because of cross-linking, degradation, or crystallization, for instance.

### *5.2.4 UNIVERSAL TERMINAL BEHAVIOR*

The ratio of longest relaxation time $\lambda_{max}$ and characteristic experimental time defines the Deborah number [21] for the MS experiment as follows:

$$N_{De} = \frac{\lambda_{max}}{t_S} = \frac{\omega \lambda_{max}}{2\pi} \tag{23}$$

Here, the characteristic experimental time is the sampling time $t_S$ (Eq. (36)). For very low frequencies, the Deborah number becomes very small, $N_{De} \ll 1$, and the polymer shows its distinct behavior as liquid or solid.

#### 5.2.4.1 Polymeric Liquids

The low-frequency asymptotes of the moduli define the zero shear viscosity of the liquid

$$\eta_0 = \lim_{\omega \to 0} \frac{G''}{\omega} \tag{24}$$

and the recoverable compliance

$$J_e^0 = \frac{1}{\eta_0^2} \lim_{\omega \to 0} \frac{G'}{\omega^2} \tag{25}$$

For such low-frequency experiments, the polymer behavior is dominated by a representative longest mode $\langle\lambda\rangle$

$$\overset{0}{G}(t) \approx g_0 e^{-t/\langle\lambda\rangle} \tag{26}$$

with

$$\langle\lambda\rangle = \frac{\sum_{i=1}^{\infty} g_i \lambda_i}{\sum_{i=1}^{\infty} g_i} \tag{27}$$

in discrete representation. The dynamic moduli approach the classic terminal behavior for $N_{De} \ll 1$:

$$G'(\omega) \sim \omega^2, \qquad G''(\omega) \sim \omega \tag{28}$$

(see [8]). No new material parameters need to be introduced.

#### 5.2.4.2 Polymeric Solids

The low-frequency asymptotes of the moduli define the equilibrium modulus

$$G_e = \lim_{\omega \to 0} G' \tag{29}$$

and a transient shear viscosity

$$\eta_s = \lim_{\omega \to 0} \frac{G''}{\omega} \tag{30}$$

which determines viscous losses in solids during transient deformations.

### 5.2.5 *TYPICAL EXPERIMENTAL RESULTS*

A wide range of dynamic mechanical data on liquids and solids can be found in the classical textbooks of Ferry [8] and Tschoegl [22]. Here we can only show a few typical examples.

The typical features of dynamic mechanical data of polymeric fluids express themselves most distinctly in the special case of narrowly distributed, linear, flexible polymers of high molecular weight. Polystyrene is a good example (see Figure 5.9 in which the data shown are the starting point for finding the BSW

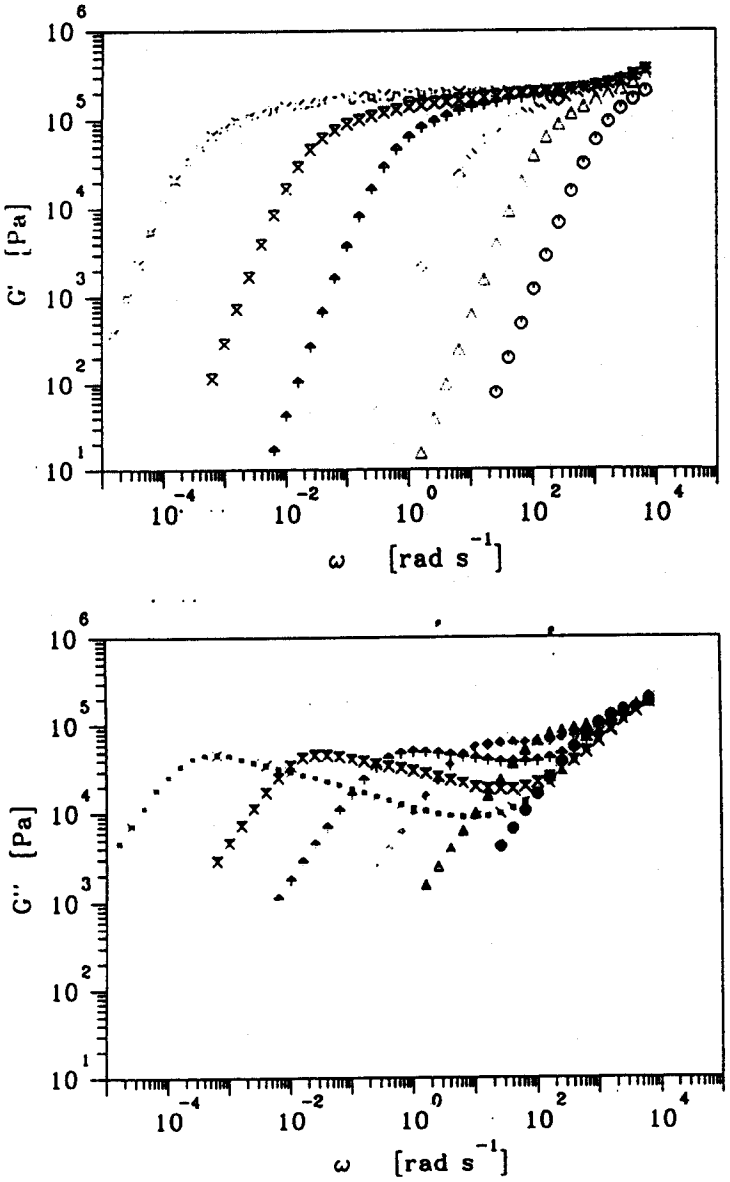


**Figure 5.9** Storage modulus $G'(\omega)$, loss modulus $G''(\omega)$, and phase shift $\delta(\omega)$ of narrowly distributed polystyrene at 180 °C. The molecular weights are 34,000; 65,000; 125,000; 292,000; 757,000; 2,540,000. Data from Schausberger *et al.* [23].

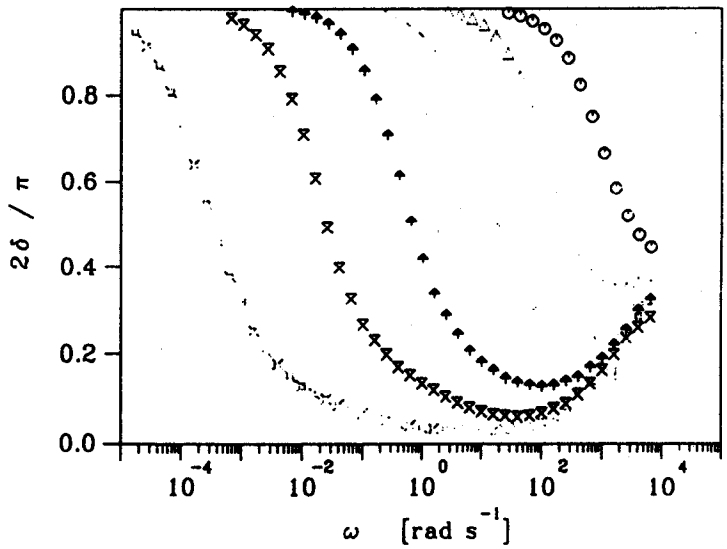


**Figure 5.9** Continued.

spectrum, Eq. (6)). At low frequencies, the typical liquid behavior of $G'(\omega_j) \sim \omega^2$ and $G''(\omega_j) \sim \omega$ can be seen. The crossover from terminal behavior to entanglement occurs at a characteristic frequency that decreases with molecular weight

$$\omega_c \sim M_w^{-z} \quad \text{with} \quad z \approx 3.4 \tag{31}$$

For model polymeric liquids of Figure 5.9, the crossover from flow to entanglement behavior results in an actual intersect of $G'$ and $G''$; the intersect frequency $\omega_x$ often serves as the inverse of a representative longest relaxation time $\lambda^*_{max} = 1/\omega_x$.. This representative time constant is somewhat smaller than the longest relaxation time $\lambda^*_{max} < \lambda_{max}$ but has the advantage that it can be read directly from $G'$, $G''(\omega)$ graphs.

The entanglement plateau of $G''(\omega)$, called the plateau modulus $G^0_N$, is known to be independent of molecular weight $M_w$. The upturn of the moduli in Figure 5.9. at high frequencies marks the crossover to the glass transition, which does not significantly depend on $M_w$.

A mixture of two polymers of different molecular weights exhibits two distinct entanglement regions [25, 24]. An example is shown in Figure 5.10. Each of the components is narrowly distributed; broadening of the molecular weight

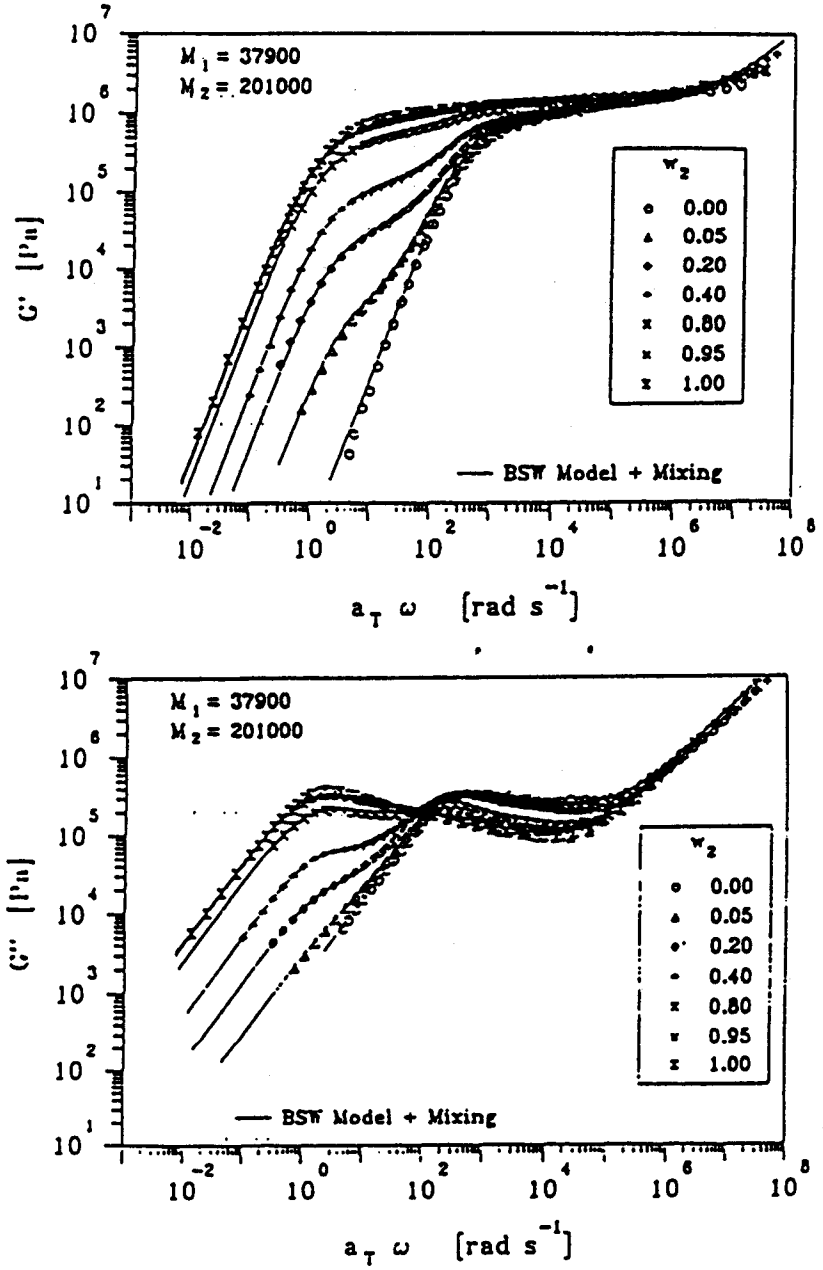


Figure 5.10 The (a) storage and (b) loss moduli of bidisperse polybutadiene (PBD) blends measured at 28 °C. The line through the data represents the model spectrum described by Jackson and Winter [24]. Both $M_1$ and $M_2$ are highly entangled.

distribution would widen the crossover regions, and the distinct features of the dynamic moduli would get lost [26].

### 5.2.6 *INTERRELATION WITH RELAXATION MODULUS AND SPECTRUM*

Experimental data of dynamic moduli $G'(\omega)$ and $G''(\omega)$ carry all the information needed to determine the relaxation modulus $\overset{0}{G}(t)$. However, extraction of the information requires the inversion of integrals

$$\text{storage modulus} \quad G'(\omega) = \omega \int_0^\infty dt\ \overset{0}{G}(t) \sin(\omega t) \tag{32}$$

$$\text{loss modulus} \quad G''(\omega) = \omega \int_0^\infty dt\ \overset{0}{G}(t) \cos(\omega t), \tag{33}$$

which is a nontrivial task. It will be discussed in Section 5.3. The above equations can be derived by inserting Eq. (16) into Boltzmann's equation of linear viscoelasticity, Eq. (4) (see, for example, Bird *et al.* [27]). The dynamic moduli may also be expressed with the continuous spectrum $H(\lambda)$ by

$$G'(\omega) - G_e = \int_0^\infty \frac{d\lambda}{\lambda} H(\lambda) \frac{(\omega\lambda)^2}{1 + (\omega\lambda)^2} \tag{34}$$

$$G''(\omega) = \int_0^\infty \frac{d\lambda}{\lambda} H(\lambda) \frac{(\omega\lambda)}{1 + (\omega\lambda)^2} \tag{35}$$

The spectrum covers the transient part of the relaxation process. This is why the equilibrium modulus needs to be subtracted when performing spectroscopy on solids.

### 5.2.7 *SPECTROSCOPIC NATURE OF EXPERIMENT*

The basic advantages of small-amplitude oscillatory strain (shear or extension) come through its spectroscopic nature: The experimental time for taking a single data point, called sampling time $t_s$, is roughly equal to the period of the strain wave

$$t_s = 2\pi/\omega \tag{36}$$

This allows measurement of specific relaxation modes with time constants on the order of $1/\omega$ independent of any longer or shorter modes that might be present in the polymer, i.e., only a small fraction of the spectrum is actually sampled in an individual experiment. Each data point $\omega_s$, $G'(\omega_s)$, $G''(\omega_s)$ is dominated by the

specific relaxation modes with relaxation times near $\lambda = 1/\omega_s$. Other relaxation modes have less influence, which can be demonstrated most efficiently with a polymer at its gel point for which the longest relaxation time diverges to infinity, $\lambda_{max} \to \infty$ [7]. Any measurement that depends on $\lambda_{max}$ will necessarily fail at the gel point. Mechanical spectroscopy, however, is able to probe intermediate modes of the spectrum without interference from the diverging $\lambda_{max}$. The spectrum at the gel point is known to be self-similar at times larger than some material characteristic crossover time $\lambda_0$ [6, 7].

$$H(\lambda) = a\lambda^{-n} \quad \text{for} \quad \lambda_0 < \lambda < \infty \tag{37}$$

For the purpose of demonstrating the spectroscopic nature of MS, we select a sampling frequency $\omega_s$ within the self-similar region of the spectrum ($\omega_s \ll 1/\lambda_0$) and evaluate the corresponding dynamic moduli by inserting Eq. (37) into Eqs. (34) and (35):

$$G'(\omega_s) = a\omega_s^n \int_0^\infty dx\, F(x) \quad \text{with} \quad F(x) = x^{-(n+1)} \frac{x^2}{1+x^2} \tag{38}$$

$$G''(\omega_s) = a\omega_s^n \int_0^\infty dx\, F''(x) \quad \text{with} \quad F''(x) = x^{-(n+1)} \frac{x}{1+x^2} \tag{39}$$

The areas under the $F$ and $F''$ curves determine the values of the complex moduli $G'$, $G''$ (see Figure 5.11). The graph shows that the relaxation modes near $\lambda\omega_s = 1$ determine the outcome of the experiment. Note that $G_e$ is equal to zero at the gel point and needs not to be considered in this example. The self-similar spectrum of the critical gel allows calculation of dynamic moduli

$$G' = a\omega^n \pi/(2 \sin(n\pi/2)) \tag{40}$$

$$G'' = a\omega^n \pi/(2 \cos(n\pi/2)) \tag{41}$$

for $\omega < 1/\lambda_0$.

This spectroscopic property needs to be contrasted with nonspectroscopic methods that measure steady-state properties (the steady shear viscosity, for instance). They simultaneously probe an integral over all relaxation modes.

### 5.2.8 *RHEOMETER GEOMETRIES*

For the most widely used configuration, the plate-and-plate rheometer (Figure 5.12), the polymer is molded into a disk-shaped sample of, for instance, radius $R$ = 12.5 mm and $h$ = 1-mm height. The sample is sandwiched between disk-shaped rheometer fixtures. The configuration has a common symmetry axis. When one of

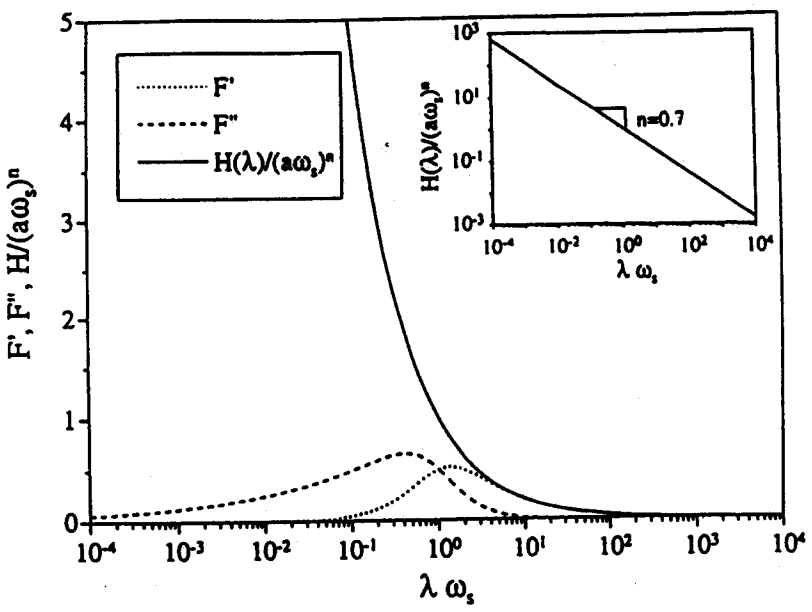


**Figure 5.11** $F(\lambda\omega_s)$ and $F''(\lambda\omega_s)$ for the evaluation of $G'$ and $G''$. Inset: reduced power law spectrum $H(\lambda) = a\lambda^{-n}$.

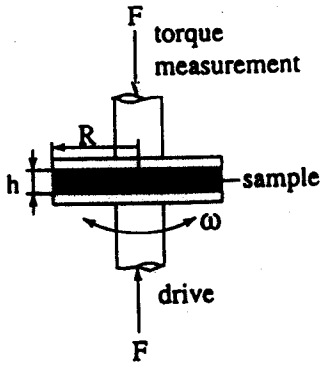


**Figure 5.12** Plate and plate rheometer with schematic of a shearing experiment with disk-shaped sample. Drive and torque measurement are on opposite sides (in this example). An axial force $F$ is required to maintain constant sample thickness $h$.

the fixtures is rotated (at constant $h$) while the other fixture is held stationary, the sample deforms and transmits a torque that can be measured. The angle of rotation and the torque can be recalculated into shear strain $\gamma(t)$ and shear stress $\tau(t)$ for further analysis. Stress and strain vary across the sample, but this does not pose a problem for experiments in the linear viscoelastic range because a linear relation exists between $\gamma(t)$ and $\tau(t)$. Large strain experiments, which we do not address here, would require Rabinowitch-type corrections or switching to other flow geometries.

Other common geometries are cone-and-plate and annulus between concentric cylinders (Couette rheometer). Detailed descriptions of the many possible geometries and related data analyses are well documented in textbooks [27–31]. Data analysis requires corrections for instrument compliance and inertia.

### 5.2.9 *EXPERIMENTAL PROBLEMS*

It seems to be the general property of polymers that they slip on surfaces [32]. However, the slip is negligibly small in most experiments. Data analysis proceeds under the assumption that there is no relative velocity between the polymer and the wall of the rheometer ("stick"). Problems arise when the slip velocity is large enough to alter the strain in the sample. Discussion of this subject would exceed the task of this chapter.

Another common problem is the lack of chemical stability of the sample. Rheological experiments require time during which the polymer may change and standard data analysis will no longer be possible. This subject is of great importance and will be discussed in Section 5.4.

The experimental frequencies range over $\omega_{min} < \omega < \omega_{max}$. Sample inertia and elastic instabilities limit the experiment at high frequencies ($\rightarrow\omega_{max}$). Transducer sensitivity (or lack thereof) and increasing sampling time $t_s \sim 1/\omega$, limit the experiment at low frequencies ($\rightarrow\omega_{min}$).

The large strain limits of the linear viscoelastic range of the experiment can be detected by Fourier analysis of the stress response to the sinusoidal strain [33–35]. While at small strain (linear viscoelastic regime), the stress response is of the same frequency as the input, and higher frequencies are not represented except for the noise in the experiment. However, at larger strain amplitudes additional frequencies start to appear in the stress response. These frequencies are multiples of the sampling frequency $\omega_s$. Most pronounced are the odd harmonies with $3\,\omega_s$, $5\,\omega_s$, $7\,\omega_s$, and higher. Discussion of these nonlinear effects is beyond the scope of this chapter.

### *5.2.10 PROBING NONEQUILIBRIUM STATES*

Mechanical Spectroscopy also allows the study of material samples that were forced away from their equilibrium state. Such nonequilibrium conditions may arise, for instance, during large strains. For the purpose of MS, one modulates the large strain by superimposing small perturbations of sinusoidal [36] or step [37] dynamics. The only requirement for MS is a linear response of the stress increments to the small strain perturbations (or vice versa), whereas the main part of the experiment is still nonlinear. The experiments are difficult to perform with sufficient accuracy, and not much data are available. The main problem seems to be that the perturbations have to be extremely small in order to maintain linear modulation conditions [38]. The probing of nonequilibrium states with MS is very appealing; more such work will be seen in the near future. The basic details of data analysis are the same as those entailed in probing equilibrium states except that one has to account for the out-of-equilibrium condition in which the Boltzmann equation, Eq. (4), does not apply any more. No separate discussion will be needed here. In the remainder of this chapter, we will assume that the material has fully equilibrated because this is the most common experimental condition.

## 5.3 Data Analysis for Mechanical Spectroscopy

In this section, we will assume that oscillatory experiments have been completed successfully, that the experiments have been analyzed, and that a $G'(\omega)$, $G''(\omega)$ data set is ready for further analysis. Many different methods have been proposed for converting the measured dynamic moduli $G'$, $G''$ into the relaxation time spectrum of the test sample [8, 1, 39–45]. Orbey and Dealy [46] have presented an overview of several of these methods. The spectrum may also be extracted from any other material function besides $G'$ and $G''$. Advanced methods have been proposed for inverting creep data (see, for example, [47, 48]). However, the focus here will continue to be on the $G'$, $G''$ data.

The solution of the inversion problem will always be a compromise. Important criteria to consider are as follows [74]:

1. Good fit of the experimental data.
2. Avoidance of overfitting. The algorithm should be able to find the optimum amount of detail that can be extracted from experimental data without producing artifacts.

3. The format of $g_i$ and $\lambda_i$ should be freely adjustable during the inversion of the data.
4. The resulting material parameters should have physical meaning.
5. Minimization of the truncation error. The data are always cut off on both sides of the frequency scale. This truncation may be the source of substantial error [49].
6. Verification of experimental data quality. The data are always inconsistent to some degree because the signal-to-noise ratios differ for $G'$ and $G''$. This may cause a substantial discrepancy between fit and data, which can be detected during data analysis.
7. For practical considerations, the relaxation modulus or the spectrum should be expressed by a function or a sum of functions that can be integrated easily in the various linear viscoelastic model calculations. This again leads us to an exponential form (Eq. (8)).
8. For practical considerations, the number of parameters should be small (for ease of use in modeling calculations and for storing material data in a database).
9. For practical considerations, the computation time should be short. All conversion methods in the literature seem to satisfy this criterion owing to the high computation speed of desktop computers.

Most problematic of these criteria is truncation. *Low* frequency data should extend into the terminal region to avoid truncation, but no characteristic limiting behavior exists at *high* frequencies; high frequency truncation is unavoidable.

### 5.3.1 METHOD OF EVALUATING $H(\lambda)$ FROM $G', G''$ DATA

Conversion methods are fairly established by now, and practitioners can choose from several options. The robust numerical algorithm of Baumgärtel *et al.* [43, 50] satisfies most of the preceding criteria. It avoids ill-posedness, which seems to be inherent in the curve fitting when too many parameters are chosen. The method is especially useful when working with complex polymeric materials because the data do not need to be extrapolated beyond the experimental frequency window (as with a Fourier transform); no material-specific empiricisms are needed. A nonlinear regression simultaneously adjusts $g_i, \lambda_i, i = 1, 2, 3 \ldots, N$ to obtain a best fit of $G', G''$. A type of regularization is achieved by systematically searching for the spectrum with the smallest number of Maxwell modes that still represents the data within the experimental error margin (parsimonious modeling). A closer fit could

be achieved, but it would not have any physical significance. The determination of the spectrum consists of four steps. The steps will be discussed separately as follows:

#### 5.3.1.1 Step 1: Experiment

The $G'$, $G''$ data set is generated in an MS experiment as described in the preceding section. The data set extends over a finite time window $1/\omega_{max} < t < 1/\omega_{min}$, which should cover at least three to four decades. If possible, the frequency window has been increased further by time–temperature superposition, as will be discussed in Section 5.5.1.

#### 5.3.1.2 Step 2: Discretization

We assume that the test sample may be represented by a unique continuous function $H(\lambda)$ sufficiently smooth to be linearized within small time intervals $[\lambda_i^-, \lambda_i^+]$ around $\lambda_i$. Baumgärtel and Winter [50] proposed a simple way of discretizing the spectrum into a set of individual Maxwell modes

$$\int_{\lambda_i^+}^{\lambda_i^-} \frac{d\lambda}{\lambda} H(\lambda) e^{-t/\lambda} \cong H(\lambda_i) e^{-t/\lambda_i} \int_{\lambda_i^+}^{\lambda_i^-} \frac{d\lambda}{\lambda} = H(\lambda_i) \Delta_i e^{-t/\lambda_i}, \tag{42}$$

each of them representing a short time interval. The size of the interval is

$$\Delta_i = \ln(\lambda_i^-/\lambda_i^+) \approx \ln \sqrt{\lambda_{i-1}/\lambda_{i+1}}. \tag{43}$$

The expressions $\lambda_i^-$ and $\lambda_i^+$ are the upper and lower time limits of the step $\Delta_i$ around $\lambda_i$. Note that $\Delta_i$ is positive because $\lambda_{i-1} > \lambda_{i+1}$ owing to the convention of starting the series (Eq. (8)) with the longest relaxation time, $\lambda_{max} = \lambda_1$. For simplicity, the step size $\Delta_i$ may be chosen as a constant. It is preferable, however, to treat $\Delta_i$ as a variable because doing so allows a closer fit of the data with fewer parameters. With this discretization, the relaxation modulus becomes (see also Eq. (8))

$$\overset{0}{G}(t) - G_e = \int_0^\infty \frac{d\lambda}{\lambda} H(\lambda) e^{-t/\lambda} = \sum_{i=1}^{N} \int_{\lambda_i^+}^{\lambda_i^-} \frac{d\lambda}{\lambda} H(\lambda) e^{-t/\lambda} \cong \sum_{i=1}^{N} H(\lambda_i) \Delta_i e^{-t/\lambda_i} \tag{44}$$

This defines the relation between the spectrum and the strength of the Maxwell modes

$$g_i = H(\lambda_i) \ln \frac{\lambda_i}{\lambda_{i+1}}, \tag{45}$$

which appear in the discrete representation of the dynamic moduli

$$G'(\omega) - G_e = \sum_{i=1}^{N} g_i \frac{(\omega\lambda_i)^2}{1 + (\omega\lambda_i)^2} \tag{46}$$

$$G''(\omega) = \sum_{i=1}^{N} g_i \frac{\omega\lambda_i}{1 + (\omega\lambda_i)^2} \tag{47}$$

The values of $g_i$ decrease for short time intervals $\Delta_i$. This is an important fact that needs to be considered when comparing discrete spectra with each other.

The continuous spectrum can be completely reconstructed from the discrete modes if the highest frequency in the wave representation of $H(\lambda)$ (Fourier series) is smaller than twice the discretizing frequency [51]. This needs to be checked in each case, if possible. The discretizing frequency is defined as the reciprocal mode spacing $1/\Delta_i$. The discrete step size $\Delta_i$ can, however, not be arbitrarily small because of the noise in the data. We will return to these criteria when choosing the density of the discrete relaxation modes.

#### 5.3.1.3 Step 3: Determination of the Discrete Solution $g_i, \lambda_i, i = 1, 2, 3 \ldots N$

From the preceding equations, the discrete spectrum $g_i, \lambda_i, i = 1, 2, 3 \ldots N$ may be determined by fitting the measured values of the dynamic moduli.

For an experiment with $M$ data points, $[\omega_k, G'(\omega_k), G''(\omega_k)]$ with $k = 1, 2, 3, \ldots M$, the deviation between fit, Eqs. (46) and (47), and data points may be expressed as standard deviation $SD$ by

$$SD^2 = \frac{1}{M} \sum_{k=1}^{M} \left[ 1 - \frac{1}{G'(\omega_k)} \sum_{i=1}^{N} \frac{g_i(\omega_k\lambda_i)^2}{1 + (\omega_k\lambda_i)^2} \right]^2 + \left[ 1 - \frac{1}{G''(\omega_k)} \sum_{i=1}^{N} \frac{g_i\omega_k\lambda_i}{1 + (\omega_k\lambda_i)^2} \right]^2 \tag{48}$$

Minimization of $SD$ (for constant $N$) results in a parameter set $g_i, \lambda_i$ for the best fit. The fitting program first places a large number of Maxwell modes $g_{i,0}, \lambda_{i,0}$ evenly

over the frequency range of the data, including an additional frequency decade on both sides. The modes can be calculated directly by solving a system of algebraic equations. A nonlinear fit follows in which $g_i$, $\lambda_i$, and $N$ are optimized to obtain the best fit of the data with a minimum number of modes.

The right choice of $N$ is essential for the success of the algorithm. For small values of $N$, the discrete spectrum is still too coarse, and model calculations with the spectrum appear wavy. The waviness and the deviation between fit and data decrease as we take more and more modes. This is documented in Figure 5.13 in which the (minimized $\partial SD/\partial g_i, \lambda_i = 0$) standard deviation $SD$ decreases as $N$ is allowed to grow. The $SD$ curve basically consists of two arms, the steep one for the improved fit of the sample's contribution to $G'$, $G''$ and the flat one for the fitting of the noise in the data. The crossover between these two regions is where we suggest placing $N$, i.e., the value of $N$ depends on the noise level in the data. The resulting relaxation time spectrum has been termed the parsimonious spectrum [50] because it attempts the best fit with the fewest number of parameters.

The mode density *N/decade* has to be chosen such that it satisfies the Mozorov Discrepancy Principle [53] and the Nyquist theorem [51]. The Mozorov Discrepancy Principle gives an upper limit of $N$ beyond which the data fitting becomes physically meaningless. We define this limit by the mode density at the transition from material fitting to noise fitting (marked as "optimum range" in Figure 5.13). The Nyquist theorem requires that this characteristic mode density

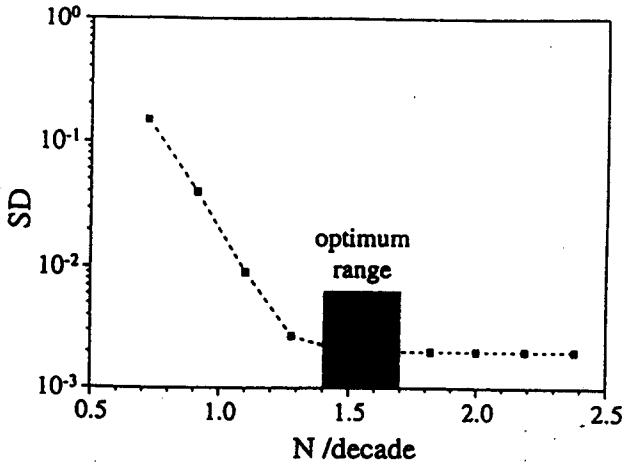


**Figure 5.13** Calculated standard deviation between data and discrete moduli (parsimonious model) Ref. [52].

(= discretizing frequency) be at least twice as high as the highest frequency in the wave representation of $H(\lambda)$. This requirement normally is satisfied because (1) good experiments have little noise and, thus, give reasonably high values for the characteristic mode density and (2) the spectrum $H(\lambda)$ is a very gradually changing function (for most materials).

Higher discretizing frequencies would reconstruct the high-frequency variations (noise) in the data [51]. It would be possible to use higher discretizing frequencies and avoid noise reconstruction by introducing additional smoothing assumptions. These assumptions, however, can easily produce artifacts that are difficult to identify. We purposely avoid this phenomenon with the parsimonious modeling.

The calculated relaxation spectrum may be directly converted into the retardation spectrum $j_i$, $\Lambda_i$, $i = 1, 2, 3 \ldots (N-1)$, as reported by Baumgärtel and Winter [43, 18].

The calculated discrete set of parameters $g_i$ and $\lambda_i$ (also $j_i$ and $\Lambda_i$) is, obviously, only valid in a time window that corresponds to the frequency window of the input data $t_{min} \cong 1/\omega_{max}$ and $t_{max} \cong 1/\omega_{min}$. However, in cases where the terminal time of the material is known (longest relaxation mode for liquids or equilibrium modulus for solids), the upper time limit becomes irrelevant and, in turn, the discrete spectra become valid for infinitely long times (zero frequency).

#### 5.3.1.4 Step 4: Conversion of the Discrete Solution in a Continuous Spectrum

As the last step, the discrete spectrum needs to be converted back into the continuous spectrum with points $H(\lambda_i) = g_i/\Delta_i$ on the continuous line $H(\lambda)$ (see the example of Figure 5.14).

The preceding result has been achieved without any prior smoothing of the data. The data are expressed with a minimum of parameters and within the *SD* of the data. The information is extracted from the data to the fullest extent without over-interpretation of the data, which would lead to unacceptable artifacts.

### *5.3.2 PROPERTIES OF THE SOLUTION*

After having completed the solution procedure, we are ready to explore the properties of the solution algorithm. This exploration is the most interesting part of working on a computer algorithm because it most likely will lead to unexpected

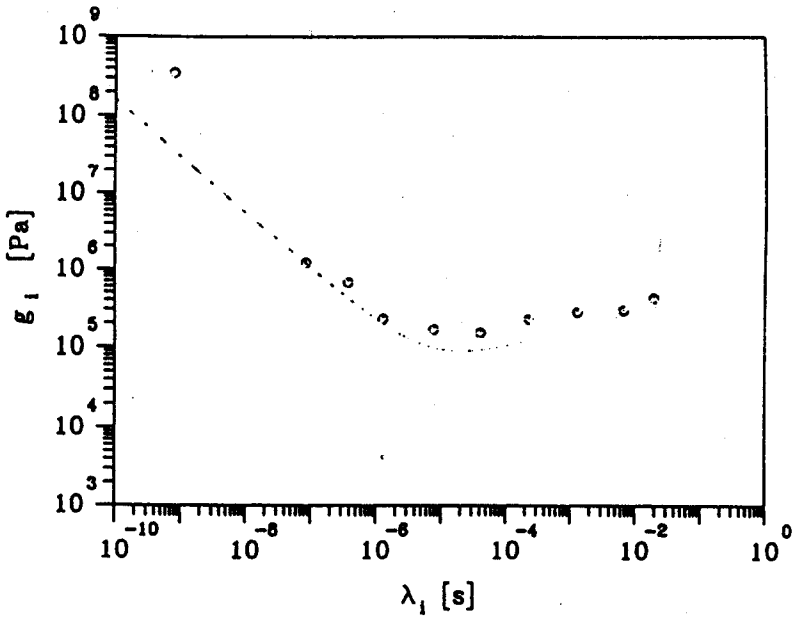


**Figure 5.14** Discrete relaxation time spectrum as calculated from dynamic mechanical data of a nearly monodisperse linear polybutadiene with $M_w$ = 70,000. The line represents the continuous BSW spectrum for the same material.

results that long for explanation just as in a real experiment. We start out by searching for general trends in the behavior of the algorithm and then try to abstract these trends into general statements ("rules") and check the limits at which they start to fail. Some of these properties will be discussed in the next paragraphs, and often it will become clear that our observations will need more rigorous proof before they will be acceptable in a more general context.

#### 5.3.2.1 Ill-Posedness

The inversion of a *single* integral equation such as Eq. (22) for $G'$ (or Eq. (23) for $G''$) is known to be an ill-posed problem [54, 40]. A sign of ill-posedness would be large variations in the solution when adding (or omitting) some data or even a single data point to the experimental set. Little is known about the simultaneous inversion of *two* interrelated integrals. A surprising observation, contrary to statements in the literature, is that the typical characteristics of ill-posedness completely vanish

when the preceding inversion is simultaneously performed on both integrals for $G'$ and $G''$. This lack of ill-posedness is most valuable for our purposes of finding the spectrum.

Ill-posedness has been avoided with discrete relaxation spectra by keeping $N$ small [54]. The algorithm of Baumgärtel *et al.* also becomes more robust when reducing $N$. However, robustness does not seem to be the problem, for the algorithm behaved well-posed up to high $N$ values as long as data were artificially smoothed (smoothing for testing purposes only), see Figure 16 in Ref. [50]. An upper limit occurred naturally at very high $N$ at which the modes are so dense that rounding errors become important in the minimization procedure. This suggests that it is not the ill-posedness that creates an upper limit on $N$, but it is the over-fitting of noise in the data.

#### 5.3.2.2 Uniqueness

It will be necessary to show uniqueness before further physical conclusions can be drawn from any experimental spectrum. For checking uniqueness, one needs to transform the discrete spectra $g_i, \lambda_i$ into continuous form to see that, indeed, various very different looking discrete spectra reduce to the *same continuous function* $H(\lambda)$. If this is satisfied, we call the discrete solutions unique because they are all equivalent representations of one and the same $H(\lambda)$.

Several additional observations let us believe that the parsimonious spectrum poses a "unique" solution to the problem (within experimental error). The various observations entail the following:

1. The starting set $g_{i,0}, \lambda_{i,0}$ does not affect the final parsimonious spectrum.
2. Random omission of several data points from the experimental input does not change the calculated continuous $H(\lambda)$.
3. Addition of some artificial, random noise to the data does not affect the calculated continuous $H(\lambda)$ provided that we maintain the approximate overall noise level.

In addition to these observations on real data, Baumgärtel *et al.* [43, 50] produced artificial $G', G''$ data from a known spectrum $H(\lambda)$ and, to close the circle of thought, used the algorithm as described above and always returned to the original spectrum. This is an important test that needs to be satisfied by a conversion algorithm before considering it further.

### 5.3.3 *COMPUTER-AIDED CONSISTENCY TESTS*

#### 5.3.3.1 Prediction of Other Material Functions and Comparison with Experiment

The newly determined $H(\lambda)$ may be expressed in any of the other linear viscoelastic material functions [8] and the result should be consistent with experimental observations and with theory. The most obvious tests are

plotting of $G'$, $G''$ data against calculated $G'$, $G''$ (from $H(\lambda)$),
plotting of deviations between the preceding functions versus frequency,
plotting of relaxation modulus (from $H(\lambda)$),
plotting of creep compliance (from $H(\lambda)$), and
predicting of stress during start-ups and comparison with experiments (see equations in Section 5.6).

All of these tasks are commonly performed by computer, and the result is presented in the interactive graphics mode. Specific tests are discussed in the following paragraphs.

##### *5.3.3.1.1 Kramers–Kronig Check [74]*

The storage modulus $G'$ and the loss modulus $G''$ are not independent of each other. They are interrelated by the Kramers–Kronig relation

$$\frac{G'(\omega)}{\omega^2} = \frac{2}{\pi}\int_0^\infty \frac{dx}{x}\frac{G''(x)}{\omega^2 - x^2}, \tag{49}$$

which has been described by Bird *et al.* [27] and by Boij *et al.* [55]. The relation is difficult to apply to experimental data because the data are truncated at low and high frequency. This is where discretization helps. The discrete form of Eq. (49)

$$\sum_{i=1}^{N}\frac{g_i\lambda_i^2}{1+(\omega\lambda_i)^2} = \frac{2}{\pi}\int_0^\infty dx\ \frac{1}{\omega^2 - x^2}\sum_{i=1}^{N}\frac{g_i\lambda_i}{1+(\omega\lambda_i)^2} \tag{50}$$

may be rearranged into

$$\sum_{i=1}^{N} g_i\lambda_i\left\{\frac{\lambda_i}{1+(\omega\lambda_i)^2} - \frac{2}{\pi}\int_0^\infty dx\ \frac{1}{\omega^2 - x^2}\frac{I}{1+(x\lambda_i)^2}\right\} = 0 \tag{51}$$

It can be shown that the function in the bracket is equal to zero for any $\lambda_i$ because each individual Maxwell mode $g_i$, $\lambda_i$ satisfies the Kramers–Kronig relation. The

equilibrium modulus $G_e$ is included in these calculations as a Maxwell mode with infinitely long relaxation time. The conclusion is that the discrete relaxation modulus, Eq. (8), will always satisfy the Kramers–Kronig relation.

This result has far-reaching implications for the evaluation of dynamic mechanical experiments because the spectrum calculation tells us when a data set went bad: If the computer algorithm is not able to fit a given set of $G'$, $G''$ data, then one can assume that the data set violates the Kramers–Kronig relation. Such violation can always happen for various experimental reasons. We have used that criterion effectively for detecting faulty data sets. The Kramers–Kronig check is one of the very strengths of the parsimonious spectrum calculation.

### *5.3.4 COMPUTER CODE*

The preceding data analysis has been written as computer code. The code is used by many laboratories worldwide. Detailed descriptions can be found through the Internet at http://members.tripod.com/~Rheology/.

## 5.4 Time-Resolved Mechanical Spectroscopy (TRMS)

Mechanical spectroscopy is the preferred tool to study materials with changing structure such as polymers during gelation (an example will be given later), phase transition, decomposition, polymerization, and so forth. Time-resolved techniques were developed to study the dynamic properties of such mutating materials [56, 57, 58, 19]. We use the term mutation as a general expression for changes that affect the molecular mobility and thus the relaxation behavior of the investigated material. The change in chemically cross-linking polymers depends on the extent of reaction $p$, which changes from $p = 0$ to $p \to 1$ as the reaction proceeds. For want of a generally applicable variable, we will use symbol $p$ to identify the structural state of a changing material without specifying the type of structural change.

The linear viscoelastic behavior of a transient material may be expressed as

$$\tau(t) = \int_{-\infty}^{t} dt' \overset{t}{\underset{t'}{G}}(t, t', p(t'))\, \dot{\gamma}(t') \tag{52}$$

where $\tau(t)$ is the shear stress and $\dot{\gamma}(t)$ is the shear rate. The relaxation function $\overset{t}{\underset{t'}{G}}(t, t', p(t'))$ accounts for mutation during the relaxation processes. It is positively valued and decays monotonically with $s = t - t'$. The equation is based on the linear superposition principle of stress and strain, i.e., its range of validity is restricted to sufficiently small strains and strain rates.

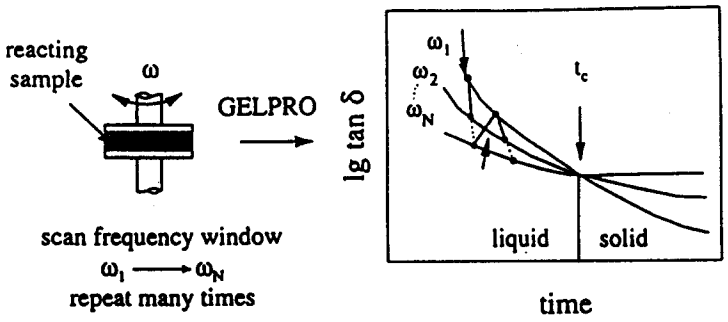


**Figure 5.15** Schematic of time-resolved mechanical spectroscopy and expected data for a cross-linking material. The data analysis is performed with a software called GELPRO. Reference [19].

Mechanical spectroscopy is applicable to transient samples, especially because of its spectroscopic nature. However, a wide range of frequencies needs to be applied either simultaneously [20] or sequentially. Simultaneous probing at several frequencies (multiwave method, Fourier transform mechanical spectroscopy) has the advantage of shortening the experimental time and accommodating higher rates of mutation. However, it has the disadvantage that the overall strain amplitude may quickly exceed the limits of linear viscoelasticity. For this reason, we recently used sequentially increasing frequencies, one after the other, just as in conventional MS. At each frequency a single measurement was performed. This frequency cycle was then repeated again and again until the rate of mutation ceased. A schematic of this technique is shown in Figure 5.15 for a cross-linking material. In this example, the point of liquid–solid transition can be determined from the crossover of $\tan\delta(\omega)$, as described by Chambon and Winter [6]. A real data set is shown in Figure 5.16.

The sampling time $t_s$ in time-resolved MS (TRMS) is again the duration of a single measurement, i.e., the time required by the rheometer to take a single data point. For an oscillatory shear experiment, $t_s$ is approximately given by the period of the imposed shear wave (Eq. (36)). During this period the shear stress response is measured continuously and then transformed into a single data point for the properties of interest in such an experiment; for example, the dynamic moduli $G'$ and $G''$.

### 5.4.1 *QUASI-STABILITY*

The sample changes during each sampling. If the total change is large during $t_s$, the function $\overset{t}{G}$ of Eq. (52) needs to be known for the data analysis (which rarely is the case). To avoid such problems of sample mutation, the mutation during

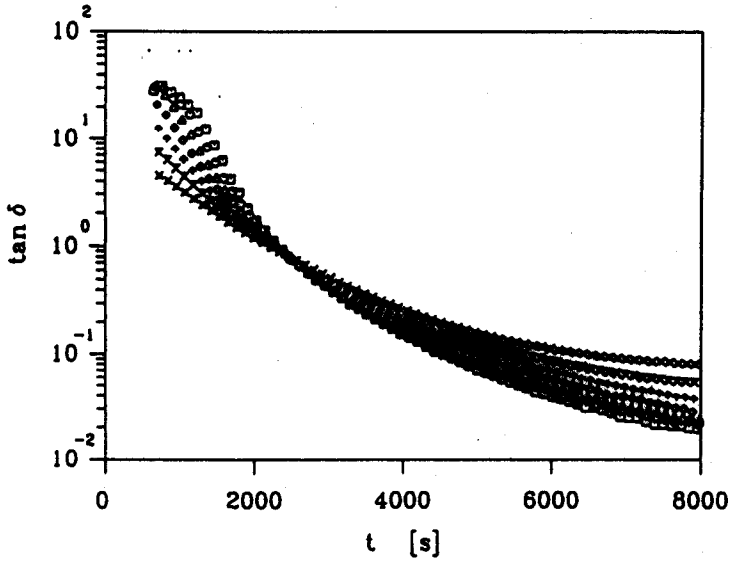


**Figure 5.16** Evolution of loss tangent ($\tan\delta$) during cross-linking of PBD38 at 28 °C for several frequencies (1–100 rad/s, 3 frequencies/decade). The gel point is marked by the $\tan\delta$ crossover, i.e., the frequency independence of $\tan\delta$. Reference [73].

$t_s$ needs to be small enough so that it can be neglected. The rate of mutation is shown as slope in Figure 5.17. The inverse of the slope has been used to define a mutation time $\lambda_{mu}$, which may refer to the properties $G'$ or $G''$

$$\lambda'_{mu} = \left|\frac{1}{G'}\frac{\partial G'}{\partial t}\right|^{-1}, \quad \text{or} \quad \lambda''_{mu} = \left|\frac{1}{G''}\frac{\partial G''}{\partial t}\right|^{-1} \tag{53}$$

The total change during the sampling time $t_s = 2\pi/\omega$ has been expressed in the mutation number [59] by

$$N_{mu} = \frac{\text{experimental time}}{\text{mutation time}} = \text{experimental time} * \text{rate of change},$$

which needs to be evaluated for both $G'$ and $G''$ as follows:

$$N'_{mu} = \frac{2\pi}{\omega G'}\frac{\partial G'}{\partial t}, \quad \text{or} \quad N''_{mu} = \frac{2\pi}{\omega G''}\frac{\partial G''}{\partial t}, \tag{54}$$

the larger value determines the admissibility of the experiment. Usually, $G'$ responds more sensitively for transient materials. The mutation number may be

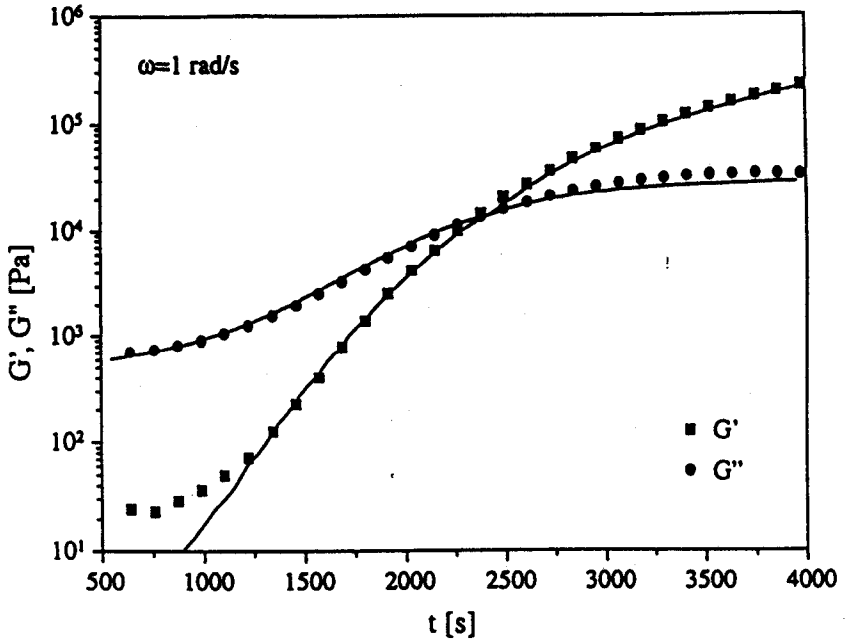


**Figure 5.17** Evolution of dynamic moduli during cross-linking of PBD38 at $\omega = 1$ rad/s ($T = 28$ °C). Lines represent the model calculations as outlined in this chapter, and symbols depict the experimental data.

combined with the Deborah number (Eq. (23)) by

$$N_{De}N'_{mu} = \frac{\lambda}{G'}\frac{\partial G'}{\partial t}, \quad \text{or} \quad N_{De}N''_{mu} = \frac{\lambda}{G''}\frac{\partial G''}{\partial t} \tag{55}$$

This dimensionless group is important because dynamic mechanical experiments become nonlinear when $N_{mu}$ or $N_{mu}$ $N_{De}$ exceed certain values. Winter *et al.* [59] found, for instance, that nonlinear effects in a gelation experiment could be observed for $N_{mu}$ greater than 0.15. On the other hand, Mours and Winter [19] determined a critical mutation number of 0.9 for a constant heating rate experiment. For $N_{mu}$ or $N_{mu}$ $N_{De}$ below the critical value, the sample can be assumed to behave quasi-stably during the sampling of single experimental points.

The characterization of a quasi-stable sample can be understood by looking at the schematic plot (property $G'$, $G''$ versus time on different time scales) in Figure 5.18. The material properties change during the entire mutation. If the probing time or the rate of overall property change is small, the sample behaves quasi-stably during the experimental time $t_s$, resulting in a sinusoidal stress response

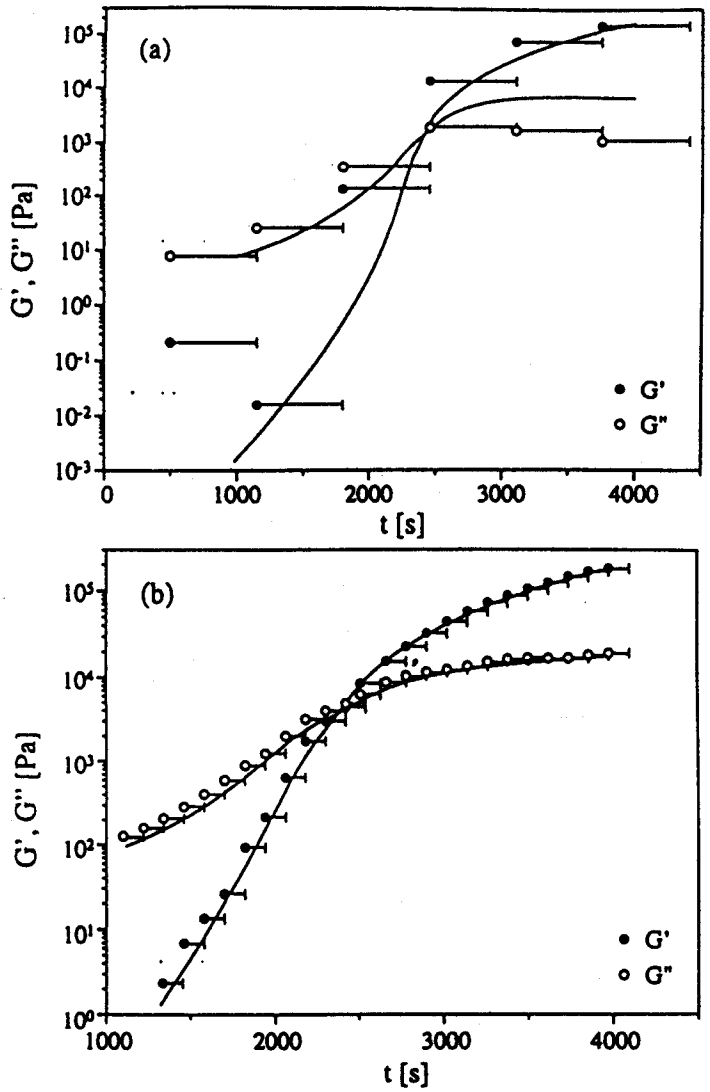


**Figure 5.18** Evolution of dynamic moduli during cross-linking of PBD38 at (a) $\omega = 0.01$ rad/s and (b) $\omega = 0.1$ rad/s ($T = 28$ °C). Moduli calculated from the modeled shear stress are depicted by symbols. The displayed range is equivalent to the experimental time $t_s$. Lines correspond to the phenomenological model of Mours and Winter [73].

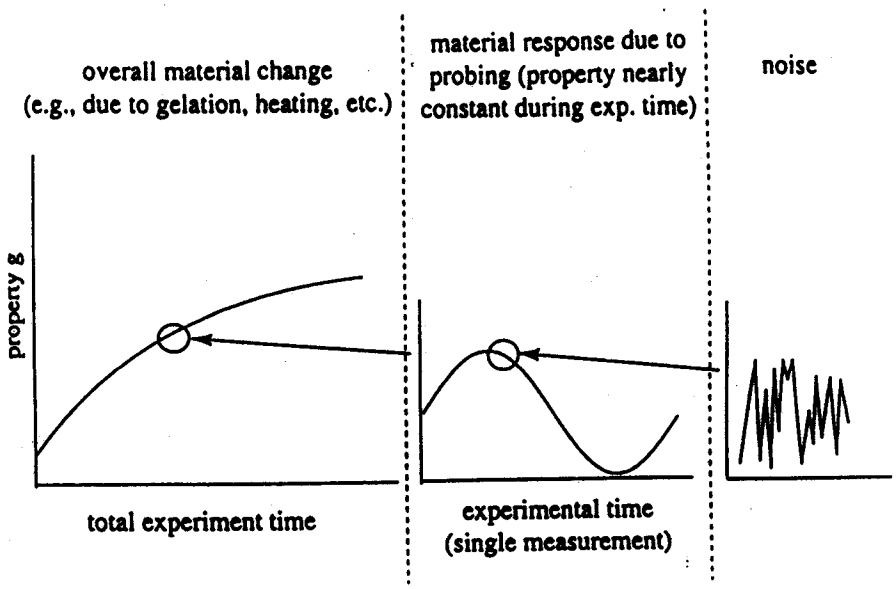


**Figure 5.19** Change of interesting property $g$ on different time scales (left: change of property during overall experiment; middle: response to the probing at prescribed frequency (during experimental time $t_s$); right: rapid variations of experimental signal (noise)) [19].

to an imposed sinusoidal strain. In this case, each data point represents a distinct (quasi-stable) state of the material.

### *5.4.2 TRMS DATA ANALYSIS [19]*

Each TRMS data point represents a different state of the material, and interpolation is necessary to obtain the desired data as a function of frequency at distinct material states. The interpolation requires the following sequence of procedures, which have been assigned to a personal computer:

#### 5.4.2.1 Sorting

The data points $G'(\omega_j, p(t))$ and $G''(\omega_j, p(t))$ $(j = 1, 2, \ldots M$, where $M$ is the number of discrete frequencies), initially sorted in terms of increasing time, must be rearranged in terms of increasing frequency.

#### 5.4.2.2 Smoothing

Continuous curves $f_j'(p)$ and $f_j''(p)$ are calculated for each frequency $\omega_j$ representing the evolving moduli $G'(\omega_j, p(t))$ and $G''(\omega_j, p(t))$ as a function of the variable $p$, which describes the ongoing mutation process. Data smoothing in conjunction with the curve fitting gives the most consistent results. This must be repeated for each discrete frequency $\omega_j$ of the $G'$ and $G''$ data set.

#### 5.4.2.3 Interpolation

Using these fitted curves, dynamic mechanical material functions ($G'(\omega, t_i)$, $G''(\omega, t_i)$, $\tan\delta(\omega, t_i)$, $2\delta(\omega, t_i)/\pi$, etc.) can be interpolated at discrete material states (represented by the time $t_i$) for each of the frequencies. This results in a comprehensive rheological description of each material state during the structural or other development that influences the flow properties.

#### 5.4.2.4 Further Analysis

The interpolated data sets can now be used to study the material behavior at different structural states. One example is the use of superposition principles, if applicable, such as time–temperature superposition or time–cure superposition, to combine the data into master curves. As an example for a typical TRMS experiment, data on a cross-linking polybutadiene [73] are shown in Figure 5.20.

### *5.4.3 CROSS-LINKING OF POLYBUTADIENE (PBD 38)*

As an example, we consider cross-linking of a polybutadiene precursor with $M_w = 37{,}900$ (PBD38). The evolution of the relaxation time spectrum during cross-linking was described using a phenomenological model and corresponding parameters, as given by Mours and Winter [73]. Mutation numbers for all frequencies were calculated using

$$N_{mu} = \frac{t_s}{G'}\frac{\partial G'}{\partial t},$$

as given in Table 5.1. The very low mutation numbers ($N_{mu} < 0.07$) at the experimental frequencies ($\omega > 1$ rad/s) ensured that effects of the material change on the measured dynamic moduli were negligible. In these cases, agreement between the model calculations and the experimental dynamic moduli was satisfactory, as displayed in Figure 5.17, for the case of $\omega = 1$ rad/s. The deviations at short times in the storage modulus are due to the transducer insensitivity at low torque values.

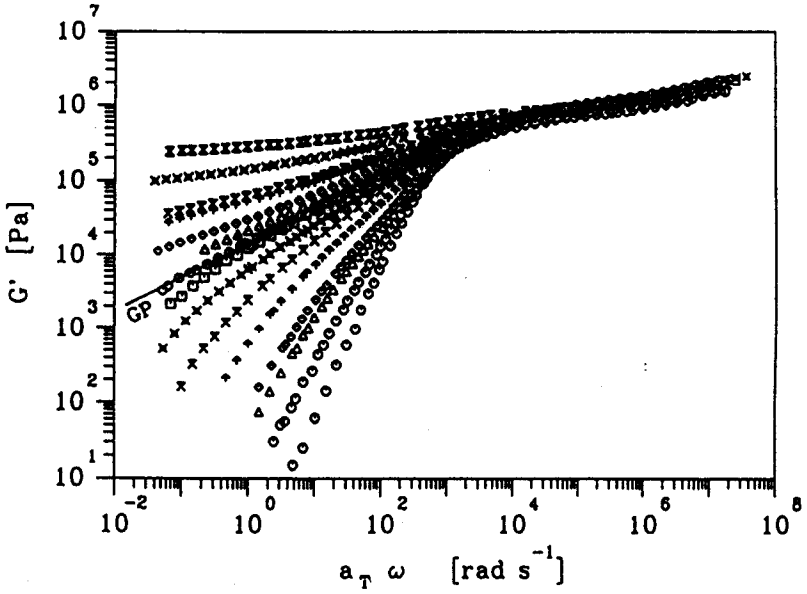


**Figure 5.20** Storage modulus data of PBD38 samples at different extents of reaction ($T_{ref} = 28$ °C). Time-resolved mechanical spectroscopy data in combination with data on chemically stopped samples extend the frequency window, which, for TRMS alone, would be quite small. The gel point is marked by a line [73].

The resulting dynamic moduli for the lower frequencies ($\omega = 0.01$ rad/s and $\omega = 0.1$ rad/s) are shown in Figure 5.18. Two sets of symbols are displayed for each frequency connected by horizontal lines. The reason for this is the ambiguity in determining the time for each data point. Because the experimental time $t_s$ can be rather long, depending on the frequency (see Table 5.1), the calculated

*Table 5.1* Average and maximum mutation numbers and experimental times at several frequencies during cross-linking of PBD38.

| $\omega$ (rad/s) | $t_s(s)$ | $N_{mu,max}$ | $N_{mu,average}$ |
|---|---|---|---|
| 0.01 | 650 | 3.7 | 2.1 |
| 0.03 | 300 | 3.0 | 1.2 |
| 0.05 | 200 | 2.1 | 0.9 |
| 0.1 | 120 | 1.1 | 0.5 |
| 1 | 10 | 0.07 | 0.03 |
| 10 | 3 | 0.02 | 0.01 |

values represent an average over this time period $t_s$. In an actual experiment, the rheometer usually uses the initial time of $t_{initial}$ ($t_s = t_{end} - t_{initial}$) as the actual time for the corresponding data point. This results in an overestimation of the moduli because they keep increasing during the cross-linking reaction. Similarly, if one takes $t_{end}$ as time for the data point, the moduli are generally too low. The lines in the preceding figures represent model calculations of the dynamic moduli using the phenomenological model developed by Mours and Winter [73].

Calculated moduli agree reasonably well with experimental data, except for the lowest frequency cases ($\omega = 0.01$ rad/s). The average and maximum mutation numbers are very high (above 2) in this case. For the three higher frequencies ($\omega = 0.03$ rad/s to $\omega = 0.1$ rad/s), the moduli increase monotonically with time and follow along the expected values. However, because of the ambiguity in the determination of the time $t$ for each data point, it is impossible to find actual agreement between simulation and model. Lower mutation numbers (at higher frequencies) tend to give closer agreement. This is especially true beyond the gel point, where mutation numbers are usually lower than before the gel point. The criterion $N_{mu}$ tends to take on the highest value shortly before the gel point for all studied frequencies.

In conclusion, the preceding modeling basically agrees with experimental findings that the mutation number during time-resolved rheometry experiments of cross-linking samples should stay below a value of 0.2. The average value of 0.5 at $\omega = 0.1$ rad/s is still too high to achieve good agreement with the expected data without arbitrarily changing the time stamp of each data point. However, the lower mutation number at frequencies above $\omega = 1$ rad/s results in good agreement between experimental data and simulation.

## 5.5 Temperature Effects and Time–Temperature Superposition

### *5.5.1 TIME–TEMPERATURE SUPERPOSITION (tTS)*

Thermorheologically simple materials obey the so-called time–temperature superposition principle for which time and temperature changes are equivalent [8]. Frequency-dependent data at different temperatures can be superimposed (by simultaneous horizontal and vertical shifting) to yield a so-called master curve at a reference temperature $T_{ref}$ within the experimental temperature range. This property was found with homopolymers (and some miscible blends) over wide frequency or time windows. Commercial software packages are available that can

easily perform this type of shifting on a personal computer (see, for instance, http://members.tripod.com/~Rheology/). The superposition typically yields plots of

| | |
|---|---|
| reduced storage modulus $b_T G'$ | versus reduced frequency $a_T \omega$ |
| reduced loss modulus $b_T G''$ | versus reduced frequency $a_T \omega$ |
| loss tangent $G''/G'$ | versus reduced frequency $a_T \omega$ |
| reduced relaxation modulus $b_T \overset{0}{G}$ | versus reduced time $t/a_T$ |
| reduced dynamic viscosity $b_T \eta^*/a_T$ | versus reduced frequency $a_T \omega$ |

The temperature shift factors $a_T$ and $b_T$ represent the horizontal and vertical shift, respectively, of data at the experimental temperature and onto $T_{ref}$.

Time–temperature superposition allows shifting of discrete spectra to new temperatures. This requires that groups of discrete relaxation modes

$$\lambda_i(T) = \lambda_i(T_{ref})a_T, \qquad \text{and} \quad g_i(T) = g_i(T_{ref})/b_T \tag{56}$$

shift with common shift factors $a_T$ and $b_T$. Time–temperature superposition, if applicable, is able to extend the available frequency window (see Figure 5.21). This extension of the frequency window is one of the main reasons for performing time–temperature superposition.

### 5.5.2 *LIMITS OF tTS*

An understanding of tTS behavior in MS experiments helps to define experimental criteria for measuring the limits when tTS starts to break down. For example, temperature changes may induce transitions in morphology that cause sudden changes in the molecular mobility. Appropriate methods for MS have been discussed in Section 5.4. Time–temperature superposition is not possible for these materials.

It should be noted that even the long-chain dynamics (entanglement and terminal region) of homopolymers do not necessarily shift with the same shift factor as the short segmental dynamics (glass transition, glass), as shown by Inoue *et al.* [60]. This is not very obvious because most data sets do not cover a wide enough frequency or time window. In general, miscible polymer blends do not obey the tTS. Exceptions are polymer blends for which (a) the glass transition temperatures of the components are very close to each other, or (b) the molecules of the blend components interact very strongly, or both [61, 62].

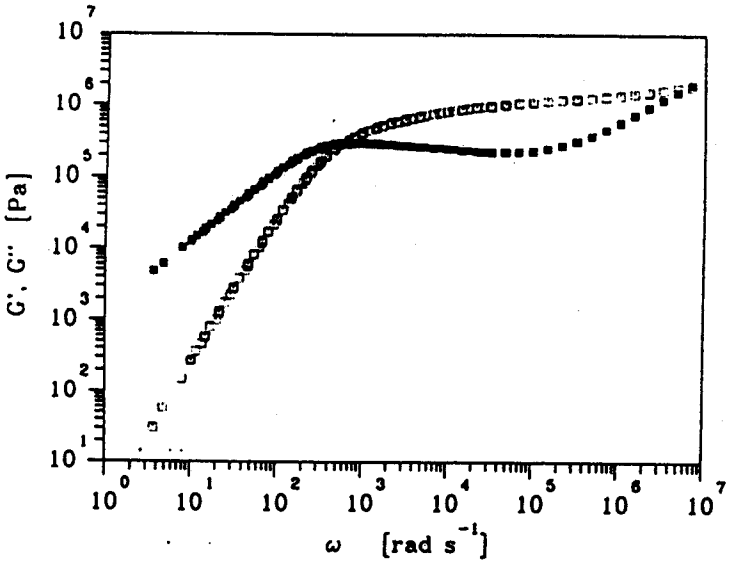


**Figure 5.21** Storage and loss modulus master curves of a nearly monodisperse linear polybutadiene with Mw = 37,700. The data cover the terminal region at low frequencies and show the entanglement plateau in $G'$ at intermediate frequencies and the crossover to the glass transition at high frequencies [72].

### 5.5.3 *TEMPERATURE SHIFT FACTORS*

Relaxation rates are highest at high temperatures. There have been different attempts in the literature to describe the temperature dependence of the horizontal shift factors. Today, the three-parameter Williams–Landel–Ferry equation (WLF) is widely accepted [8]:

$$\log a_T = \frac{-C_1(T - T_{ref})}{C_2 + T - T_{ref}}, \qquad T_g < T < (T_g + 200\,\mathrm{K}), \tag{57}$$

where $T_g$ is the glass transition temperature of the specific polymer. Williams *et al.* [63] proposed universal values of $C_1 = 7.60$ and $C_2 = 227.3$ K if $T_{ref}$ is chosen somewhat close to $T_g$.

Some researchers prefer the format of the three-parameter Vogel equation [64, 65]:

$$\ln a_T = \frac{E_a}{R}\left(\frac{1}{T - T_V} - \frac{1}{T_{ref} - T_V}\right), \tag{58}$$

which is equivalent to the WLF equation. The Vogel temperature $T_V$ is much below the glass temperature. Parameters in Eqs. (57) and (58) are convertible into each other:

$$C_1 = \frac{E_a}{R(T_{ref} - T_V)} \quad \text{and} \quad C_2 = T_{ref} - T_V \tag{59}$$

Far above the Vogel temperature, $T \gg T_V$, a simpler two-parameter Arrhenius-type expression is sufficient to trace experimental data:

$$\ln a_T = \frac{E_a}{R}\left(\frac{1}{T} - \frac{1}{T_{ref}}\right) \qquad \text{for } (T_g + 200\,\text{K}) < T. \tag{60}$$

The Arrhenius parameter $E_a/R$ is usually extracted from a plot of $\log a_T$ versus reciprocal temperature $1/T$. If the Arrhenius-type dependence is a valid approximation, this plot shows a straight line with a slope of $E_a/(2.303R)$. In the case of WLF-behavior, the temperature dependence of $a_T$ deviates from this straight line (see Figure 5.22 for polybutadiene with $M_w = 37{,}900$).

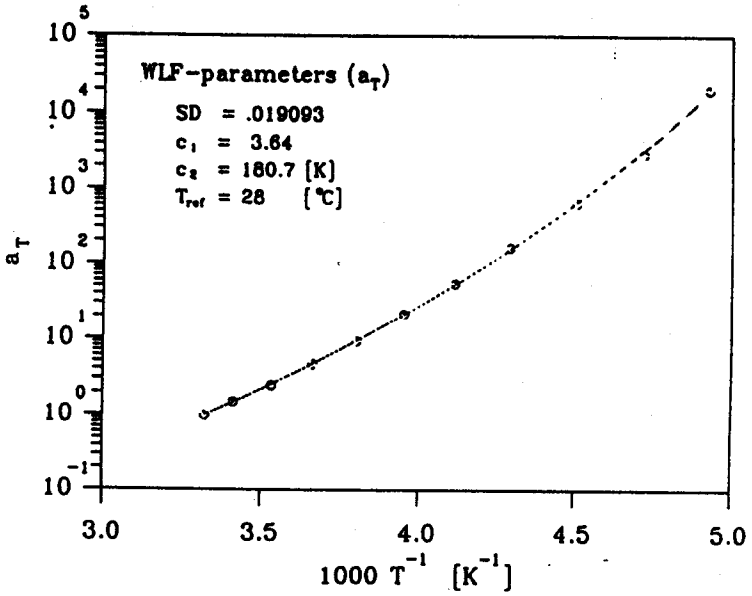


**Figure 5.22** Horizontal temperature shift factors $a_T$ and WLF-fit for PBD38. Reference [73].

Temperature-induced density changes result in a vertical shift factor [8]

$$b_T(T; T_{ref}) = \frac{T_{ref}\rho(T_{ref})}{T\rho(T)} \tag{61}$$

Its value is usually close to unity for moderate temperatures differences.

Time–temperature superposition of experimental data yields values of shift factors $a_T$ and $b_T$ at different temperatures so that the necessary parameters of Eqs. (57), (58), and (60) can be evaluated by regression techniques. If the parameters $E_a/R$, $C_1$, $C_2$, $T_V$, and $\rho(T_{ref})/\rho(T)$ are known, the constructed master curve can be shifted to any temperature within the experimental range. Extrapolation of shift factors to temperatures outside the experimental window is possible but should be viewed with caution.

### 5.5.4 *NONISOTHERMAL FLOW*

Processing flows are rarely isothermal, and the temperature variations severely influence the stress. Hopkins [66] and Morland and Lee [67] suggested a simple modification of the memory integral equations to account for nonisothermal histories $T(t') \neq T_{ref}$. The Boltzmann's equation, Eq. (4), may be rewritten as

$$\tau(t) = \int_{-\infty}^{t} dt' \dot{\gamma}(t') \sum_{i=1}^{N} g_i \, e^{-f(t;t')/\lambda_i} \tag{62}$$

with an exponent

$$f(t; t') = \int_{t'}^{t} dt'' \frac{1}{a_T(t'')} \tag{63}$$

The temperature shift factor changes along the path line of material elements according to their temperature history $a_T(t'') = a_T(T_{ref}; T(t''))$. The nonisothermal effects result in a stretching or compressing of the time scale. Conveniently, one uses $f(t; t')$ as the new time. For isothermal flow, $f$ reduces to $f = t - t'$. It should be noted that Eqs. (62) and (63) only apply to polymers for which the tTS principle holds.

### 5.5.5 *TEMPERATURE SCAN*

The temperature dependence of molecular mobility in polymers can be measured by gradually increasing (or decreasing) temperature during small-amplitude

oscillatory shear. This so-called temperature sweep or temperature scan (TS) is a commonly used experiment in polymer rheometry. The frequency $\omega$ is held constant throughout and, hence, the experiment has been called isochronal TS (although it is only isochronal with respect to the experimental time scale; the probed material time scale changes with temperature). The choice of frequency is quite arbitrary and limits the observation to molecular motions in the vicinity of a single mode instead of a wider spectrum of relaxation times. The TS experiment is not very informative for this reason.

In extension of this common procedure, the rheometer should be programmed to probe, while heating a polymer sample, a sequence of frequencies $\omega_i$ within a frequency window $\omega_{min} < \omega_i < \omega_{max}$. The sequence of frequencies may be repeated cyclically during the temperature scan. The method requires that the sample be in thermal equilibrium at all times, which seems to be the case for many rheometers even at moderate-to-high heating rates [19]. In this fashion, a single experiment provides the temperature and frequency dependence of the relaxation spectrum. The problem is that every data point in this experiment, which can be called frequency–temperature scan (FTS), is taken at a new temperature, and data analysis requires interpolation. However, such data interpolation methods and their limits of application are well established (time-resolved rheometry, see Section 5.4). Modern rheometers allow a similar procedure, the FTS. In this experiment, the polymer sample is probed at a cyclically repeated sequence of frequencies. After each frequency sequence, the temperature is increased or decreased in preprogrammed steps. Furthermore, one can perform several independent frequency scans at different temperatures to achieve the desired frequency and temperature-dependent data.

## 5.6 Applications of the Relaxation Time Spectrum

The relaxation spectrum describes the underlying features of all linear viscoelastic material functions (except for the equilibrium modulus $G_e$ in solids). It contains all necessary information about the relaxation behavior and therefore represents a complete rheological picture of the material within the linear viscoelastic regime. Many different material functions can be directly calculated from the spectrum. For example, a dynamic mechanical experiment with data sets $G'(\omega)$ and $G''(\omega)$ may be converted into $\overset{0}{G}(t)$ and compared with the results from a stress relaxation experiment, $\overset{0}{G}(t)$. Similarly, MS and creep experiments can be compared and scrutinized for self-consistency. The MS data may be converted into a spectrum

that defines the zero-shear viscosity $\eta_0$ and first normal stress coefficient $\psi_1$:

$$\eta_0 = \int_0^\infty d\lambda H(\lambda) = \sum_{i=1}^{N} g_i \lambda_i \tag{64}$$

$$\psi_1 = 2\int_0^\infty d\lambda\, \lambda H(\lambda) = 2\sum_{i=1}^{N} g_i \lambda_i^2 \tag{65}$$

### 5.6.1 *LINEAR VISCOELASTIC SIMULATIONS*

The spectrum allows for the simulation of start-up of shear or extensional flow in a sample that had been equilibrated at rest. Simulation involves the tensorial form of the Boltzmann equation, see Appendix 5.A, which can be found in rheology text books. For example, in a start-up and stress relaxation experiment, a material is sheared initially with a constant strain rate $\dot{\gamma}_0$ for a time $t_0$. The strain is then kept at a constant value. During this experiment, the stress is recorded. In the linear viscoelastic region, the shear stress $\tau(t)$ and the first normal stress difference $N_1(t)$ response during the initial shear, $0 < t < t_0$, is given by [1]:

$$\tau(t) = \dot{\gamma}_0\left[G_e t + \sum_{i=1}^{N} g_i(1 - e^{-t/\lambda_i})\right] \tag{66}$$

$$N_1(t) = \dot{\gamma}_0^2\left[G_e t^2 + 2\sum_{i=1}^{N} g_i \lambda_i^2 (1 - (1 + t/\lambda_i)e^{-t/\lambda_i})\right]$$

and during stress relaxation ($t_0 < t$)

$$\tau(t) = \dot{\gamma}_0\left[G_e t_0 + \sum_{i=1}^{N} g_i \lambda_i \left(e^{-(t-t_0)/\lambda_i} - e^{-t/\lambda_i}\right)\right] \tag{67}$$

$$N_1(t) = \dot{\gamma}_0^2\left[G_e t_0^2 + 2\sum_{i=1}^{N} g_i \lambda_i^2 (1 - (1 + t_0/\lambda_i)e^{-t_0/\lambda_i})e^{-(t-t_0)/\lambda_i}\right]$$

Another example is the start-up of uniaxial extension at constant rate $\dot{\varepsilon}_0$. The first normal stress difference is predicted as [68]:

$$\tau_{11} - \tau_{22} = \sum_{i=1}^{N} g_i \left[\frac{1 - 2\dot{\varepsilon}_0\lambda_i e^{-(1-2\dot{\varepsilon}_0\lambda_i)t/\lambda_i}}{1 - 2\dot{\varepsilon}_0\lambda_i} - \frac{1 + \dot{\varepsilon}_0\lambda_i e^{-(1+\dot{\varepsilon}_0\lambda_i)t/\lambda_i}}{1 + \dot{\varepsilon}_0\lambda_i}\right] \tag{68}$$

### 5.6.2 *FLOW MODELLING*

The spectrum has been used in commercially available programs to simulate the flow behavior of viscoelastic materials at large strains (for example, simulation

software using finite element methods to study the flow in complex geometries). The spectrum is an important part of large-strain constitutive equations [27, 69].

Flow modeling of polymer processing often relies on the steady shear viscosity $\eta(\dot{\gamma})$ when only the relaxation time spectrum is available. Fortunately, for many polymers heuristic relations exist that predict the viscosity from the linear relaxation time spectrum. An estimate of the flow curve $\eta(\dot{\gamma})$ may be based on the Cox–Merz relation [70] between the steady and dynamic viscosity:

$$\eta(\dot{\gamma}) = \eta^*(\omega)\Big|_{\omega=\dot{\gamma}} = \sqrt{G'^2 + G''^2}/\omega\Big|_{\omega=\dot{\gamma}}$$

$$= \sqrt{\left[\sum_{i=1}^{N} \frac{g_i \lambda_i^2 \dot{\gamma}}{1+(\lambda_i\dot{\gamma})^2}\right]^2 + \left[\sum_{i=1}^{N} \frac{g_i \lambda_i}{1+(\lambda_i\dot{\gamma})^2}\right]^2} \tag{69}$$

### 5.6.3 *RELAXATION PATTERNS*

A long-standing quest in polymer physics is the search for a relation of molecular architecture and linear viscoelastic properties [8, 71, 72]. Ideal molecular architectures are believed to generate some simple relaxation patterns. One example for this simplicity in pattern detection is the BSW spectrum, which describes the relaxation of a linear flexible polymer of uniform length (Eq. (6)). From all the commonly used rheological material functions, this spectrum was preferred because it allows the most simple expression for the observed relaxation phenomena. A look at the dynamic moduli $G'$ and $G''$ (as, for example, shown in Figure 5.9) does not easily reveal this simple pattern of the spectrum (Figure 5.4) that completely describes the linear viscoelastic relaxation behavior. Another example for such an ideal spectrum is found with cross-linking polymers at their gel point, Eq. (37).

## Appendix 5.A Boltzmann Equation

The linear constitutive equation of a viscoelastic material following the Boltzmann superposition principle is given by

$$\tau(t) = \int_{-\infty}^{t} dt' \overset{0}{G}(t-t')\dot{\gamma}(t') \tag{A1}$$

Various forms of the Boltzmann equation have been in use. It often is written in

terms of strain $\gamma$ between states at $t$ and $t'$

$$\gamma(t;t') = \int_{t'}^{t} dt'' \dot{\gamma}(t'') \tag{A2}$$

The Boltzmann equation is then transformed to

$$\tau(t) = \int_{-\infty}^{t} dt' \overset{0}{m}(t-t')\,\gamma(t;t') \tag{A3}$$

with the memory function $\overset{0}{m}(s)$ given by

$$\overset{0}{m}(s) = -\frac{d\overset{0}{G}(s)}{ds} \tag{A4}$$

with $s = t - t'$. The continuous spectrum may be introduced into the Boltzmann equation, Eq. (4), to obtain

$$\tau(t) = G_e \int_0^{\infty} ds\, \dot{\gamma}(t-s) + \int_0^{\lambda_{max}} \frac{d\lambda}{\lambda} H(\lambda) \int_0^{\infty} ds\, e^{-s/\lambda} \dot{\gamma}(t-s) \tag{A5}$$

Calculations with the spectrum are as convenient as with the relaxation modulus. Both need to be considered on an equal footing.

Tensorial forms of the Boltzmann equation are required for flow simulations (as shown in Section 5.6.1). These use the velocity gradient tensor $\nabla v$ and the extra stress tensor $\tau$

$$\tau = \int_{-\infty}^{t} dt' \overset{0}{G}(t-t')(\nabla v(x,t') + \nabla v(x,t')^T) \tag{A6}$$

and the Finger strain tensor $B(t;t')$ [75, 69]

$$\tau = G_e B(t;t_0) + \int_{-\infty}^{t} dt' \overset{0}{m}(t-t') B(t;t') \tag{A7}$$

No new material properties need to be introduced. $B(t;t_0)$ denotes the strain with respect to the stress-free state at equilibrium.

## Appendix 5.B Related Material Functions

The small amplitude oscillatory shear experiments can be expressed in many different ways that are all related to $G'$ and $G''$. The most common of these functions

are

| | | |
|---|---|---|
| complex modulus | $G^*(\omega) = \sqrt{G'^2 + G''^2}$ | (B1) |
| complex viscosity | $\eta^*(\omega) = \sqrt{G'^2 + G''^2}/\omega$ | (B2) |
| loss tangent | $\tan\delta = G''/G'$ | (B3) |
| dynamic viscosities | $\eta'(\omega) = G''/\omega$ and $\eta''(\omega) = G'/\omega$ | (B4) |
| stiffness | $S(\omega) = \dfrac{G'(\omega)}{\omega^{2\delta/\pi}\cos\delta \quad \Gamma(1-2\delta/\pi)}$ | (B5) |
| relaxation exponent | $n(\omega) = 2\delta/\pi$ | (B6) |
| dynamic compliances | $J'(\omega) = \dfrac{G'}{G'^2 + G''^2}$ and $J''(\omega) = \dfrac{G''}{G'^2 + G''^2}$ | (B7) |

where $\Gamma(x)$ is the gamma function.

## References


1. H. M. Laun, *Rheol. Acta* 17: 1–15 (1978).
2. Y. Einaga, K. Osaki, M. Kurata, S. Kimura, and M. Tamura, *Polym. J.* 2: 550 (1971).
3. K. Osaki, *Rheol. Acta* 32: 429–437 (1993).
4. K. Osaki, *Proc. 7th Int. Congr. Rheology*, Gothenburg: 104–109 (1976).
5. M. H. Wagner, *Rheol. Acta* 15: 136–142 (1976).
6. F. Chambon and H. H. Winter, *Polym. Bull.* 13: 499–503 (1985).
7. H. H. Winter and M. Mours, *Adv. Polym. Sci.* 134: 165–234 (1997).
8. J. D. Ferry, *Viscoelastic Properties of Polymers*, 3rd ed., John Wiley & Sons, New York, 1980.
9. P. E. Rouse, *J. Chem. Phys.* 21: 1272–1280 (1953).
10. P. G. de Gennes, *J. Chem. Phys.* 55: 572 (1971).
11. M. Doi and S. Edwards, *The Theory of Polymer Dynamics*, Clarendon Press, Oxford, 1986; M. Doi, *Chem. Phys. Lett.* 26: 269–272 (1974); M. Doi and S. F. Edwards, *J. Chem. Soc. Faraday Trans.* II 74: 1789–1832 (1978).
12. J. des Cloizeaux, *Euro. Phys. Lett.* 5: 437 (1988); *Macromolecules* 23: 4678 (1990).
13. K. S. Schweizer, *J. Chem. Phys.* 91: 5802 (1989); *J. Chem. Phys.* 91: 5822-5839 (1989); *J. Chem. Phys.* 103: 1934 (1995); *J. Chem. Phys.* 103: 6296 (1995); *J. Chem. Phys.* 106: 347 (1997).
14. S. T. Milner and T. C. B. McLeish, *Phys. Rev. Lett.* (1998).

15. M. Baumgärtel, A. Schausberger, and H. H. Winter, *Rheol. Acta* **29**: 400–408 (1990).
16. J. K. Jackson, M. E. De Rosa, and H. H. Winter, *Macromolecules* **27**: 2426–2431 (1994).
17. G. C. Berry and T. G. Fox, *Adv. Polym. Sci.* **5**: 261 (1968).
18. B. Gross, *Mathematical Structure of the Theories of Viscoelasticity*, Hermann & Cie., Paris (1953).
19. M. Mours and H. H. Winter, *Rheol. Acta* **33**: 385–397 (1994).
20. E. E. Holly, S. K. Venkataraman, F. Chambon, and H. H. Winter, *J. Non-Newtonian Fluid Mech.* **27**: 17–26 (1988).
21. M. Reiner, *Physics Today*, Jan: 62 (1964).
22. N. W. Tschoegl, *The Phenomenological Theory of Linear Viscoelastic Behavior*, Springer-Verlag, Heidelberg, 1989.
23. A. Schausberger, G. Schindlauer, and H. Janeschitz-Kriegl, *Rheol. Acta* **24**: 220 (1985).
24. J. K. Jackson and H. H. Winter, *Macromolecules* **28**: 3146–3155 (1995).
25. H. Watanabe and T. Kotaka, *Macromolecules* **17**: 2316 (1984).
26. S. H. Wassermann and W. W. Graessley, *J. Rheol.* **36**: 543 (1992); S. H. Wassermann, *J. Rheol.* **39**: 601 (1995).
27. R. B. Bird, R. C. Armstrong, and O. Hassager, *Dynamics of Polymeric Liquids*, Vol. 1, John Wiley & Sons, New York, 1987.
28. K. Walters, *Rheometry*, Chapman and Hall, London, 1975.
29. J. M. Dealy and K. F. Wissbrun, *Melt Rheology and its Role in Plastics Processing*, Van Nostrand Reinhold, New York, 1990.
30. C. W. Macosko, *Rheology: Principles, Measurements, and Applications*, VCH Publ., Inc., New York, 1994.
31. G. Marin, *Rheological Measurement*, 2nd ed., A. A. Collyer and D. W. Clegg, Eds., Chapman & Hall, London, 1998.
32. H. M. Laun, Characterization of Wall Slip of Polymer Melts and its Relevance to Polymer Processing, Proceedings of IUPAC Conference, p. 11, World Polymer Congress, Australia, 1998.
33. M. Wilhelm, D. Maring, and H. W. Spiess, *Rheol. Acta* **37**: 399–405 (1998).
34. J. A. Yosick, A. J. Giacomin, W. E. Stewart, and F. Ding, *Rheol. Acta* **37**: 365 (1998).
35. A. J. Giacomin and J. M. Dealy, *Rheological Measurement*, A. A. Collyer and D. W. Clegg, Eds., Chapman & Hall, London, 1998.
36. J. M. Simmons, *Rheol. Acta* **7**: 184–188 (1968) and R. I. Tanner and G. Williams, *Rheol. Acta* **10**: 528–538 (1971).
37. G. B. McKenna and L. J. Zapas, *Polym. Engr. Sci.* **26**: 725–729 (1986); *J. Polym. Sci., Phys. Ed.* **23**: 1647–1656 (1985).
38. L. Walker, J. Vermant, P. Moldernaers, and J. Mewis, *Rheol. Acta* (1998).
39. C. Friedrich and B. Hofmann, *Rheol. Acta* **22**: 425–434 (1983).

40. J. Honerkamp and J. Weese, *Macromolecules* **22:** 4372–4377 (1989); *Rheol. Acta* **32:** 65–73 (1993).
41. V. M. Kamath, M. R. Mackley, *J. Non-Newtonian Fluid Mech.* **32:** 119–144 (1989).
42. F. Schwartzl and A. J. Staverman, *Appl. Sci. Res. A* **4:** 127–141 (1953).
43. M. Baumgärtel and H. H. Winter, *Rheol. Acta* **28:** 511–519 (1989).
44. D. W. Mead, *J. Rheol.* **38:** 1769–1795 (1994).
45. I. Emri and N. W. Tschoegl, *Rheol. Acta* **31:** 161–174 (1993); *Rheol. Acta* **32:** 322–327 (1993); *Rheol. Acta* **33:** 60–70 (1994).
46. N. Orbey and J. M. Dealy, *J. Rheol.* **35:** 1035–1049 (1991).
47. J. Kaschta and F. R. Schwarzl, *Rheol. Acta* **33:** 530–541 (1994).
48. A. J. Staverman, F. Schwarzl, In: *Die Physik der Hochpolymeren*, Vol. 4, Springer-Verlag, Berlin, 1956.
49. J. K. Jackson, C. Garcia-Franco, and H. H. Winter, ANTEC **38:** 2438–2442 (1992).
50. M. Baumgärtel and H. H. Winter, *J. Non-Newtonian Fluid Mech.* **44:** 15–36 (1992).
51. H. Nyquist, *Trans. Amer. Inst. Electn Eng.* **47:** 617–644 (1928).
52. H. H. Winter, M. Mours, M. Baumgärtel, and P. Soskey, *Rheological Measurement*, 2nd ed., A. A. Collyer and D. W. Clegg, Eds., Chapman & Hall, London, 1998.
53. V. A. Mozorov, *Methods for Solving Incorrectly Posed Problems*, Springer, Berlin, 1984.
54. R. I. Tanner, *J. Appl. Polym. Sci.* **12:** 1649–1652 (1968).
55. H. C. Booij and G. P. J. M. Thoone, *Rheol. Acta* **21:** 15–24 (1982).
56. K. te Nijenhuis and H. Dijkstra, *Rheol. Acta* **14:** 71–84 (1975).
57. G. Marin, J. J. Labaig, and P. Monge, *Rheol. Acta* **16:** 527 (1975).
58. J. C. Scanlan and H. H. Winter, *Makrom. Chem., Makrom. Symp.* **45:** 11–21, (1991).
59. H. H. Winter, P. Morganelli, and F. Chambon, *Macromolecules* **21:** 532–535 (1988).
60. T. Inoue, H. Hayashihara, H. Okamoto, and K. Osaki, *J. Polym. Sci.* **30:** 409–414 (1992).
61. R. H. Colby, *Polymer* **30:** 1275–1278 (1989).
62. J. A. Pathak, R. H. Colby, S. Y. Kamath, S. K. Kumar, and R. Stadler, *Macromolecules* **31:** 8988–8997 (1998).
63. M. L. Williams, R. F. Landel, and J. D. Ferry, *J. Amer. Chem. Soc.* **77:** 3701–3707 (1955).
64. H. Vogel, *Physik Z.* **22:** 645–646 (1921).
65. G. S. Fulcher, *J. Amer. Cer. Soc.* **8:** 339–355, 789–794 (1925).
66. I. L. Hopkins, *J. Polym. Sci.* **28:** 631 (1958).
67. L. W. Morland and E. H. Lee, *Trans. Soc. Rheol.* **4:** 233–263 (1960).
68. H. Chang and A. S. Lodge, *Rheol. Acta* **11:** 127–129 (1972).
69. R. G. Larson, *The Structure and Rheology of Complex Fluids*. Oxford University Press, New York, 1999.
70. W. P. Cox and E. H. Merz, *J. Poly. Sci.* **28:** 619–622 (1958); D. Doraiswamy, A. M. Mujumdar, I. Tsao, A. N. Beris, S. C. Danforth, and A. B. Metzner, *J. Rheol.* **35:** 647–685 (1991); Y. G. Lin, P. W. Jin, J. C. W. Chien, and H. H. Winter, *Polymer* **30:** 831–834 (1989).

71. W. W. Graessley, *Adv. Polym. Sci.* **16**: 1–179 (1974); G. Marin, W. W. Graessley, *Rheol. Acta* **16**: 527 (1977); V. R. Raju, E. V. Menezes, G. Marin, W. W. Graessley, L. J. Fetters, *Macromolecules* **14**: 1668–1676 (1981); W. W. Graessley, *Adv. Polym. Sci.* **47**: 68 (1982); D. Pearson, *Rubber Chem. Tech.* **60**: 437 (1987).
72. M. Rubinstein, E. Helfand, and D. Pearson, *Macromolecules* **20**: 822 (1989).
73. M. Mours and H. H. Winter, *Macromolecules* **29**: 7221–7229 (1996).
74. H. H. Winter, *J. Non-Newtonian Fluid Mech.* **68**: 225–239 (1997).
75. A. S. Lodge, *Elastic Liquids*, Academic Press, New York, 1964.

**Corrections for** Mours M, Winter HH (2000) Mechanical Spectroscopy. Tanaka T, Ed, Experimental Methods in Polymer Science: Modern Methods in Polymer Research and Technology, Academic Press, San Diego CA. p. 495-546.

Change the equation

$$\sum_{i=1}^{N} \frac{g_i \lambda_i^{\,2}}{1+(\omega\lambda_i)^2} = \frac{2}{\pi}\int_0^{\infty} \frac{dx}{x} \frac{1}{\omega^2 - x^2} \sum_{i=1}^{N} \frac{g_i \lambda_i}{1+(\omega\lambda_i)^2} \qquad (50)$$

into

$$\sum_{i=1}^{N} \frac{g_i \lambda_i^{\,2}}{1+(\omega\lambda_i)^2} = \frac{2}{\pi}\int_0^{\infty} dx \frac{1}{\omega^2 - x^2} \sum_{i=1}^{N} \frac{g_i \lambda_i}{1+(x\lambda_i)^2} \qquad (50)$$

Change the equation

$$\sum_{i=1}^{N} g_i \lambda_i \left\{ \frac{\lambda_i}{1+(x\lambda_i)^2} - \frac{2}{\pi}\int_0^{\infty} \frac{dx}{x} \frac{1}{\omega^2 + x^2} \frac{1}{1+(x\lambda_i)^2} \right\} = 0 \qquad (51).$$

into

$$\sum_{i=1}^{N} g_i \lambda_i \left\{ \frac{\lambda_i}{1+(\omega\lambda_i)^2} - \frac{2}{\pi}\int_0^{\infty} dx \frac{1}{\omega^2 - x^2} \frac{1}{1+(x\lambda_i)^2} \right\} = 0 \qquad (51).$$

Change the equation

$$C_1 = \frac{E_a}{R(T_{ref} - T_V)}; \qquad C_2 = (T_{ref} - T_V) \qquad (59).$$

into

$$C_1 = \frac{E_a}{RC_2 \ln 10}; \qquad C_2 = (T_{ref} - T_V) \qquad (59).$$

Change the equation

$$\tau(t) = \dot{\gamma}_0 \left( G_0 t - \sum_{i=1}^{N} g_i (1 - e^{-t/\lambda_i}) \right) \qquad (66a)$$

into

$$\tau(t) = \dot{\gamma}_0 \left( G_0 t - \sum_{i=1}^{N} g_i \lambda_i (1 - e^{-t/\lambda_i}) \right) \qquad (66a)$$

Change the equation

$$N_1(t) = \dot{\gamma}_0^{\,2} \left( G_0 t_0^{\,2} - 2\sum_{i=1}^{N} g_i \lambda_i^{\,2} (1 - (1 + 1/\lambda_i) e^{-t/\lambda_i}) \right) \qquad (66b)$$

into

$$N_1(t) = \dot{\gamma}_0^{\,2} \left( G_0 t^2 - 2\sum_{i=1}^{N} g_i \lambda_i^{\,2} (1 - (1 + t/\lambda_i) e^{-t/\lambda_i}) \right) \qquad (66b)$$

change equation (B.5):

$$S(\omega) = \frac{G'(\omega)}{\Gamma(2\delta/\pi)\ \cos\delta\ \omega^{2\delta/\pi}} \quad \text{into} \quad S(\omega) = \frac{G'(\omega)}{\omega^{2\delta/\pi}\ \cos\delta\ \ \Gamma(1 - 2\delta/\pi)}$$